JOURNAL OF GEOPHYSICAL RESEARCH, VOL. 102, NO. B2, PAGES 3109-3129, FEBRUARY 10, 1997

Crustal structure of Edoras Bank continental margin and mantle thermal anomalies beneath the North Atlantic

A. J. Barton and R. S. White
Bullard Laboratories, University of Cambridge, Cambridge, England

Abstract. We discuss the structure of the continent-ocean transition of the Edoras Bank area of the NE Atlantic margin and the influence of the Iceland mantle plume during continental breakup. Edoras Bank lies close to the present-day limit of influence of the Iceland plume. Sequences of seaward dipping reflectors imaged on multichannel seismic profiles are well-developed over much of the margin. They form aerially extensive, dipping sheets, with individual reflectors imaged on margin-parallel profiles as laterally continuous and subhorizontal features. We interpret them as basalt flows extruded from linear fissure vents close to sea level at the time of continental breakup. A crustal velocity model for the margin was developed by travel time modeling of wide-angle refractions and reflections recorded on digital ocean bottom hydrophones and the structure confirmed by gravity modeling. Oceanic crust formed immediately after breakup is 10 km thick and exhibits classic layer 2 and layer 3 seismic velocities. The crustal thickness increases to the SE reaching 17 km beneath the continental fragment of Edoras Bank. The continent-ocean transition is dominated in the lower crust by a lens up to 8 km thick of high-velocity material (7.2–7.5 km s^{-1}), which exhibits a very low velocity gradient. It extends over a 60 km wide region beneath the seaward dipping reflectors. The high velocities and densities of the lower crust are probably caused by igneous rock with a high MgO content that underplated the margin or heavily intruded pre-existing crustal material during continental breakup. Both the addition of large quantities of melt to the margin and the subsidence curves inferred from postrift sediments sampled by Deep Sea Drilling Project (DSDP) boreholes on the margin indicate the presence of abnormally hot mantle beneath the area at the time of continental breakup. Comparison of the structure and subsidence history of the Edoras Bank margin with other areas of the NW European margin allows us to deduce the spatial extent and temporal variation of the thermal anomalies caused by the Iceland mantle plume during and following continental breakup. We find that at the time of breakup a thin layer of anomalously hot asthenospheric mantle ~150°C hotter than normal lay beneath the 2000 km long rift, extending from the Lofoten margin off Norway in the north to the Edoras Bank margin in the south. Over a period of 5–10 m.y. following the onset of rifting, the mantle thermal anomaly decayed rapidly to only 50°C or so above normal as the thin layer of abnormally hot mantle decompressed beneath the rift and produced a large pulse of magmatism.

Introduction

The continental margins of the northern North Atlantic contain huge quantities of igneous rock which were added to the crust during continental breakup. This has led to them being called "volcanic" continental margins to distinguish them from the "nonvolcanic" margins such as those off Goban Spur and Galicia Bank to the south, where only limited igneous activity accompanied continental breakup [*White*, 1992]. The igneous activity on "volcanic" margins is manifested by seaward dipping reflector sequences (sdrs) imaged on normal-incidence seismic profiles, which represent subaerially extruded basalt flows. In addition, high-velocity, high-density wedges of lower crustal material beneath the sdrs are often apparent from wide-angle seismic and gravity data: they are interpreted as igneous underplating or as heavily intruded, distended continental crust [*White and McKenzie*, 1989].

It is widely accepted that the outburst of volcanism in areas such as the northern North Atlantic is due to de-

Paper number 96JB03387.
0148-0227/97/96JB-03387$09.00

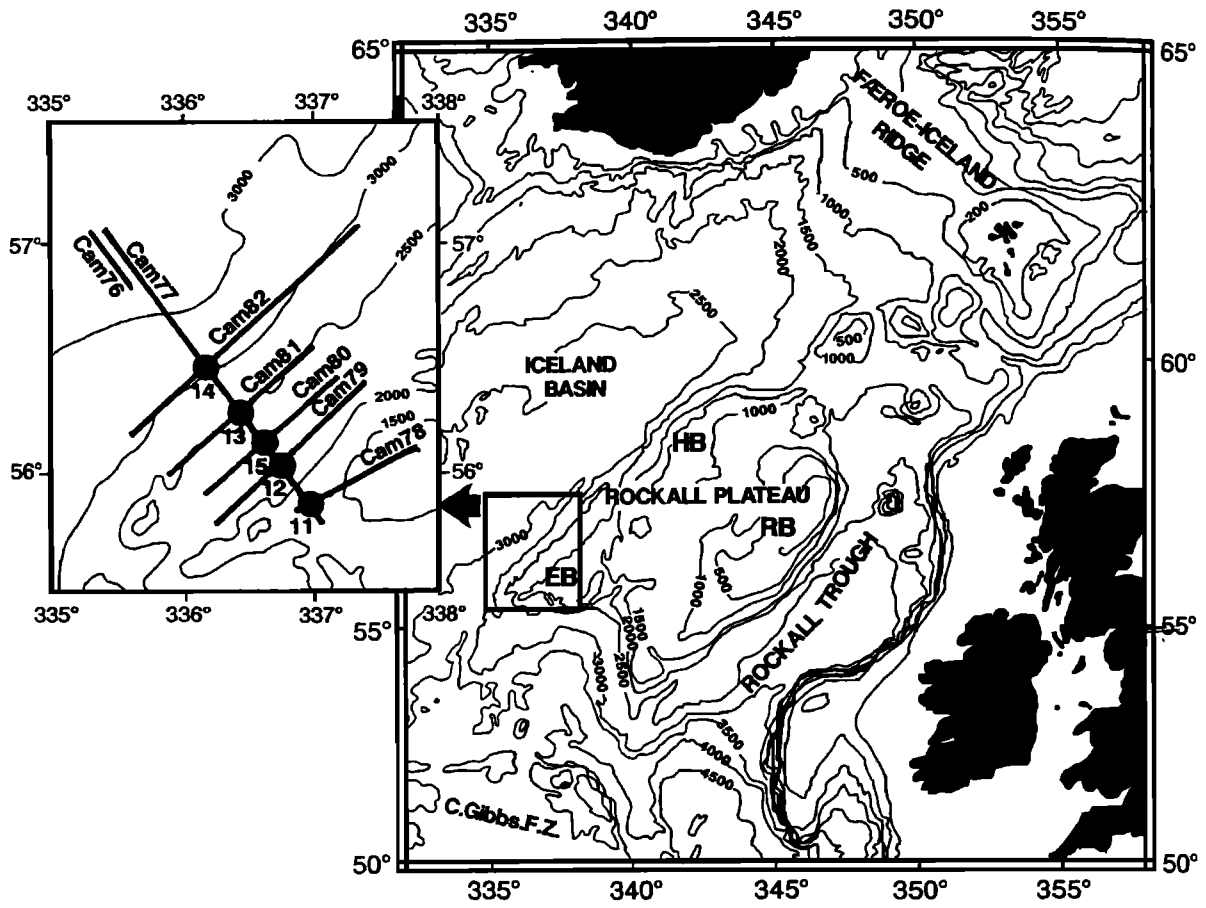

Figure 1. Bathymetry of the NE Atlantic, contoured in meters. EB, Edoras Bank; HB, Hatton Bank; RB, Rockall Bank. Inset shows locations of seismic profiles collected during CD70 in July 1992. Digital ocean bottom hydrophones are denoted by solid circles.

compression melting of underlying asthenospheric mantle which is hotter than normal due to the presence of a mantle plume [*White and McKenzie*, 1995]. However, there has been vigorous debate over issues such as whether there was active convection or passive decompression of the mantle beneath the rift and whether or not the initial extent of the high-temperature magmatism was due to a large plume head arriving directly from the core-mantle boundary.

In this paper we present results of a study of the structure of the Edoras Bank rifted continental margin, which lies close to the limit of influence of the Iceland mantle plume. We show that the plume had a profound effect on the development of the margin, despite its distal position from the center of the plume. By comparing the synrift and immediately postrift magmatic activity and subsidence history of the NW European continental margin at varying distances from the presumed plume center, we are able to constrain the shape of the thermal anomaly associated with the plume during and after continental breakup.

Geological Setting

Edoras Bank lies on the southwestern corner of the Rockall Plateau, a broad, topographically elevated region separated from the continental shelf west of Ireland by the Rockall Trough (Figure 1). Superimposed on Rockall Plateau is a series of basins and banks trending NE-SW. The Hatton-Rockall Basin separates Rockall Bank on the eastern side of the plateau from the smaller topographic highs of Hatton Bank and Edoras Bank on the western edge of the plateau.

Rockall Plateau is a continental fragment that rifted from the European continent in pre-Cretaceous times (see *Smythe* [1989] for a review). Rifting to form the Hatton-Rockall Basin probably occurred during the mid-Cretaceous. During magnetic anomaly 32–31 time (~70 Ma) spreading shifted westward to open the Labrador Sea between the Greenland-Rockall and North American blocks [*Srivastava*, 1978]. At magnetic anomaly 24R time (56–53 Ma [*Cande and Kent*, 1992]), spreading initiated between Greenland and Rockall, resulting

in the formation of a rifted continental margin along the western flank of the Rockall Plateau. The continental margin at Edoras Bank is covered by a thin veneer of mainly contourite sediment. The geophysical data set we acquired near Edoras Bank is supplemented by borehole data from Deep Sea Drilling Project (DSDP) Leg 81.

Data Acquisition

The data reported here were acquired on R.R.S *Charles Darwin* Cruise 70; 1100 km of coincident normal-incidence multichannel and wide-angle seismic data were recorded along one long (Cam77) and one short (Cam76) dip profile and on five profiles parallel to the bathymetric trend of the margin (Cam78–82) (Figure 1). Normal-incidence reflection data were recorded with a 48-channel, 2.4 km long hydrophone streamer, while wide-angle reflection and refraction data were recorded on four Cambridge digital ocean bottom hydrophones (DOBHs) located at the line intersections. The seismic source was a tuned array of 12 airguns with a total capacity of 73 l (4450 cubic inch), and a shot interval of 100 m. The two seismic methods sample different properties of the subsurface and are therefore complementary. Deep seismic reflection profiles sample the crust along predominantly vertical ray paths, creating an image which is sensitive primarily to impedance contrasts within the crust. In contrast, methods using wide-angle reflections and refractions record events at large offsets, and the crust is sampled along predominantly horizontal ray paths: such data are primarily sensitive to velocity variations. A grid of measurements of the gravitational and magnetic fields was used to constrain models of the crustal structure derived from analysis of the seismic data sets.

Normal-Incidence Seismic Data

The main dip profile, Cam77, extends from crust of continental affinity toward the top of Edoras Bank in water depths of ~1200 m, across the continental slope and over oceanic crust of the Iceland Basin where water depths exceed 3000 m. The normal-incidence profiles image two sequences of seaward dipping reflectors (Figures 2 and 3). The upper boundary of each sequence of sdrs is generally overlain conformably by a series of flat-lying and mainly parallel reflectors, although local erosion has resulted in a seaward off-lapping boundary in some places. The lower boundary of the sdr sequence is not imaged. The deepest reflectors disappear into a zone of incoherent reflections, at ~6 s two-way travel time, which obscure base-lap relationships. The sdrs reach a maximum thickness of ~4.5 km. The geometry of the sdrs is similar in each of the two sequences. Reflectors are arcuate and convex-upward. The dip of individual reflectors steepens downdip, from almost horizontal at shallow crustal levels to between 9–18° toward their base. The sdrs appear to wedge out into thin sequences landward. Their oceanward termination is more abrupt, passing from the dipping reflectors into seismically opaque basement where any crustal reflections are obscured by diffracted energy.

The three-dimensional (3D) shape of the sdrs is determined by combining dip and strike profiles. In plan view the sdrs occupy a band about 70 km wide, parallel to the bathymetric trend of the margin. Individual reflectors can be identified readily on both the

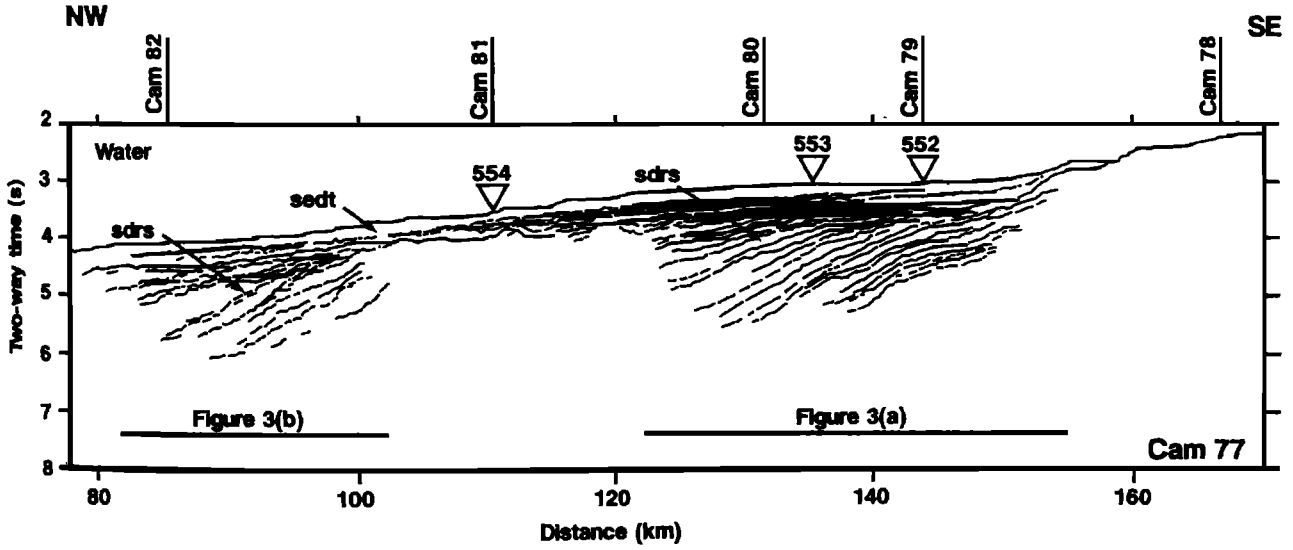

Figure 2. Line drawing of migrated normal-incidence data from Cam77. The two sequences of seaward dipping reflectors (sdrs) occur at 80–100 km and at 125–160 km. Locations of the DSDP holes 552, 553, and 554 are shown by triangles, and the intersection points of each of the strike profiles Cam78–Cam82 are labeled along the top.

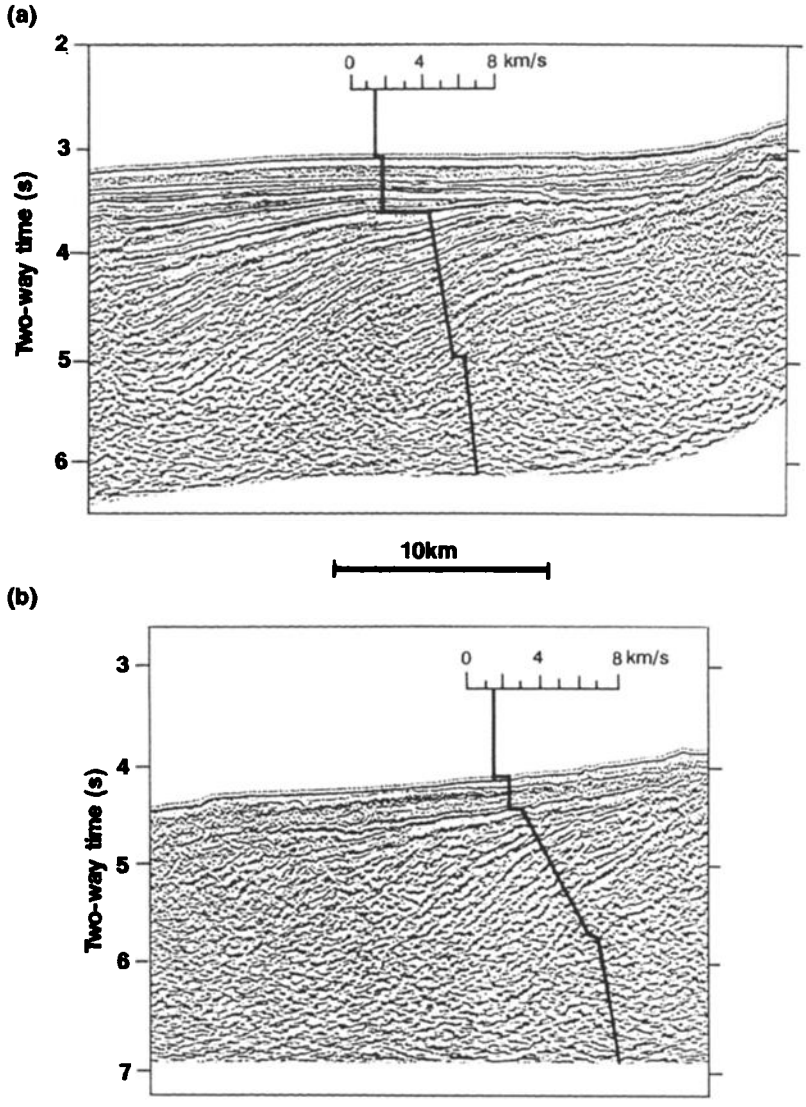

Figure 3. Detail from migrated normal-incidence profile Cam77 showing (a) the landward seaward dipping reflector sequence; (b) the oceanward seaward dipping reflector sequence (see Figure 2). *P* wave velocity profiles derived from modeling the wide-angle data are superimposed.

downdip profile Cam77 and on the strike lines Cam79 and Cam80, which intersect Cam77 through the landward sdr sequence (Figure 4). On both Cam79 and Cam80 the sdrs appear as high-amplitude subhorizontal reflectors that are laterally continuous over distances of 2 to 12 km and that generally exceed 10 km in length on Cam80. The geometry of the reflectors on both the dip and the strike lines illustrates the two-dimensional, sheet-like nature of the reflectors. The sheets strike parallel to the seafloor spreading magnetic anomaly stripes and to the bathymetric trend of the margin [*Barton and White*, 1997].

Wide-Angle Seismic Data

The DOBH recorded seismic arrivals to offsets of up to 70 km along both the strike profiles (Figure 5) and the 176 km long dip profile Cam77 (Figure 6). The signal-to-noise ratio is high at near offsets but decreases at far offsets, although phase correlation at large offsets is made possible by the dense (100 m) trace spacing. The first water bottom multiple is often of higher amplitude than the primary signal, an effect of constructive interference between the multiple and its seafloor reflection. Such enhanced signals were useful for correlating weak primary phases. The dense shot spacing produces a "wrap-around multiple" [*McBride et al.*, 1994], where primary information is obscured by noise from the previous shot. In most cases, phase correlations are visible through the multiple. In general, it is only possible confidently to correlate first arrivals and Moho reflections in the data.

Modeling Methodology

The crustal structure along dip line Cam77 was modeled as follows: (1) refractions and wide-angle reflections were picked on each record section, maintaining reciprocity and consistency between instruments; (2)

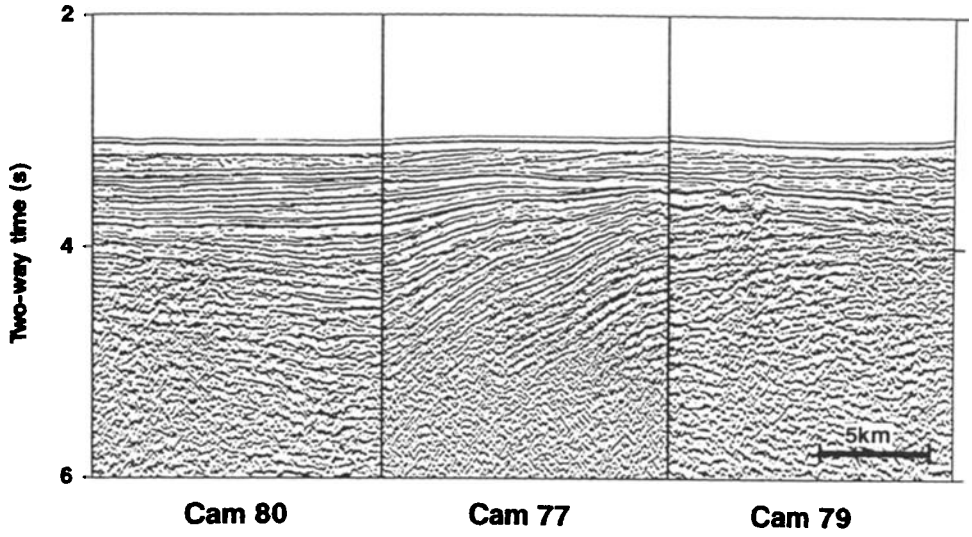

Figure 4. Unmigrated time sections from strike lines Cam79 and Cam80 and dip line Cam77. The sections are joined along their lines of intersection. Individual reflectors can be correlated between dip and strike profiles and are two-dimensional in nature.

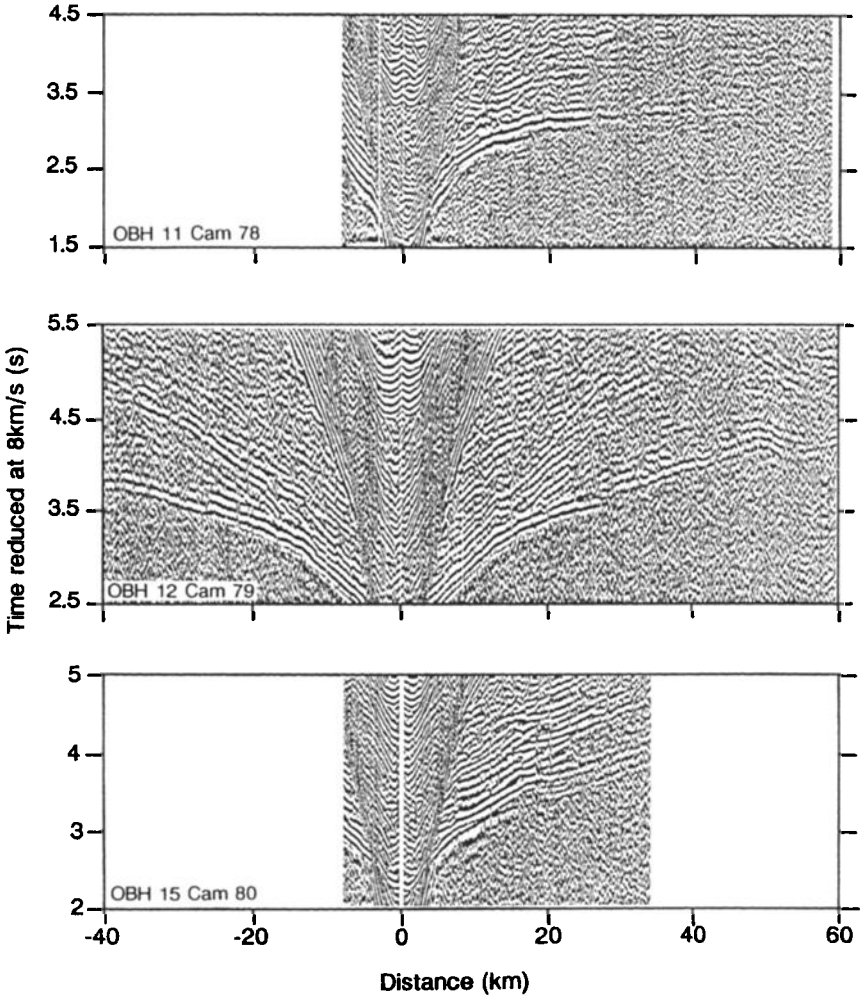

Figure 5. Record sections from DOBH11, 12, and 15 on strike lines Cam78, Cam79 and Cam80, respectively (see Figure 1 for locations). The data are band-pass filtered 5–20 Hz and reduced at 8 $km\,s^{-1}$.

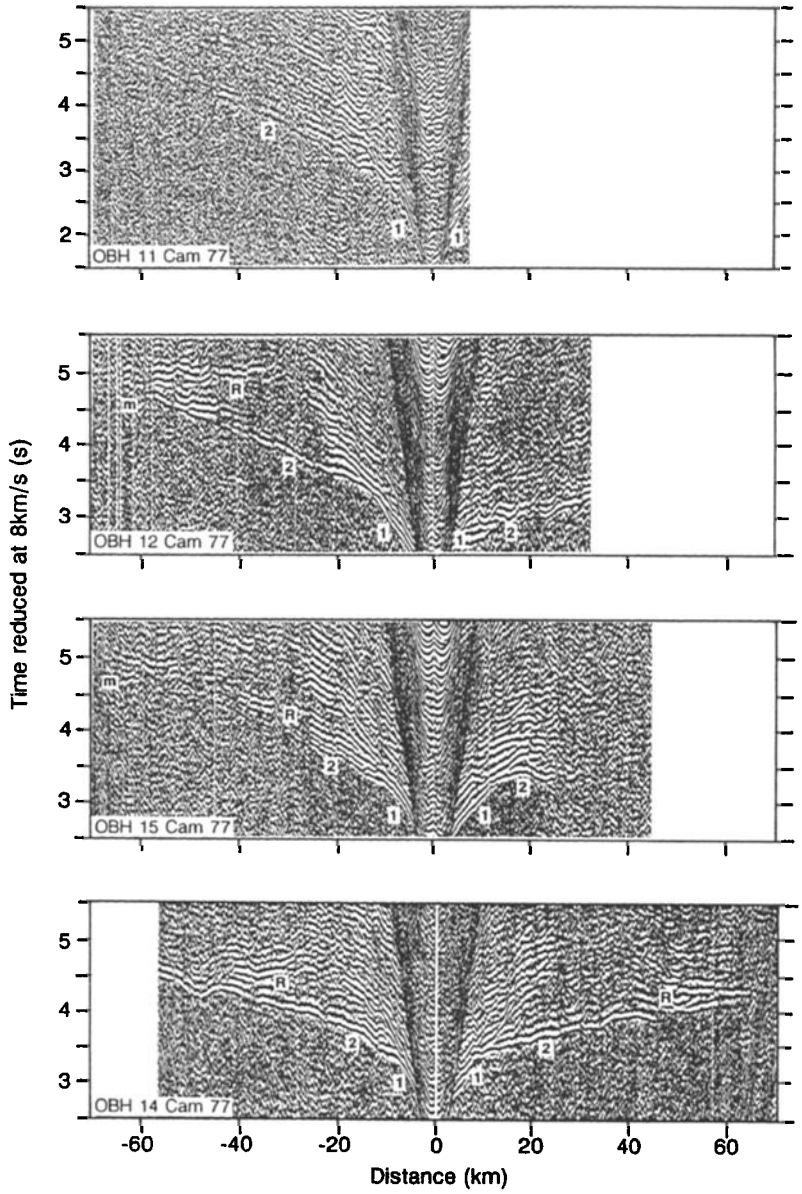

Figure 6. Record sections from DOBH11, 12, 14, and 15 on dip line Cam77 (see Figure 1 for locations). The data are band-pass filtered 5–20 Hz and reduced at 8 $km\,s^{-1}$. Annotations show the main phases: 1, 2, diving rays through the crust; m, diving rays through the mantle P_n; R, Moho reflection P_mP.

one-dimensional (1-D) models were developed at each instrument site by slope-intercept and tau-p analysis of the travel time curves; (3) initial two-dimensional (2-D) models were constructed by combining the digitized basement reflection from the multichannel profiles with bathymetry data, DSDP borehole sediment velocity data and the 1-D models; (4) travel times were modeled in 2-D by ray tracing, using the program RAYINVR [*Zelt and Smith*, 1992].

The velocity model was refined so as to minimize the misfit between the observed and calculated travel times and to ensure identical velocity structure at the crossing points of strike and dip profiles. Following forward modeling, a damped least squares inversion was made to refine the final model and to place uncertainty bounds on it. For each instrument a travel time fit was obtained for the shallowest arrivals before proceeding to deeper crustal layers. Information from each instrument was initially modeled independently until rays crossed with those from neighboring instruments and the line became reversed. Modeling of the profile then continued using all the available data. Figure 7 shows the final ray-traced model for dip line Cam77 with the observed and computed travel time curves.

Velocity Model

The final velocity model for the Edoras Bank continental margin (Figure 8) shows the following features:

1. A sedimentary layer of velocity 1.7–2.1 $km\,s^{-1}$ blankets the margin. Its thickness varies from 1300 m

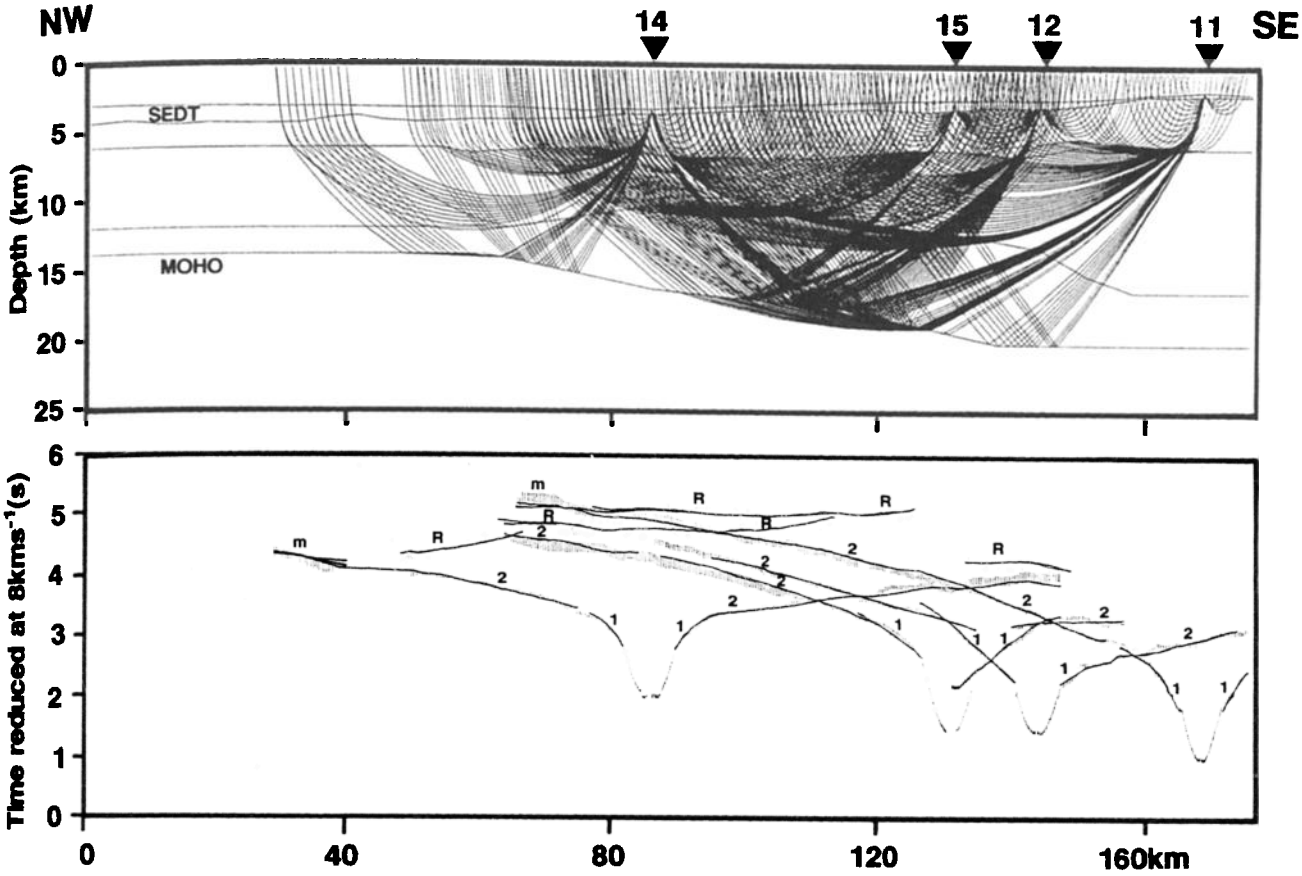

Figure 7. Ray-traced model for Cam77, with DOBH locations shown along the top. (top) Ray distribution in the final velocity model, with only one ray in every 10 shown for clarity. (bottom) Travel time picks (grey bars) and computed travel time curves (fine black lines). The height of the bar for each pick gives an estimation of the uncertainty in the travel time of that pick. Annotations show the main phases: 1, 2, diving rays through the crust; m, diving rays through the mantle P_n; R, Moho reflection P_mP.

beyond the foot of the continental slope to less than 150 m near the top of Edoras Bank. Although multichannel seismic reflection data may justify a more detailed treatment of the internal sedimentary velocity structure, our principal objectives are in the subbasement crust, and a simple sedimentary structure is adequate for that purpose.

2. The uppermost crustal layer increases in thickness from ~2.3 km beyond the foot of the continental slope to ~3.4 km in the region of the sdrs. The velocity gradient also increases from ~1 s^{-1} to ~2 s^{-1}. The velocity in the region of the sdrs is 3.0–3.5 $km\,s^{-1}$ at their top, increasing with depth to 6.0–6.5 $km\,s^{-1}$ at their base (Figure 3).

3. A midcrustal 6.5–7.2 $km\,s^{-1}$ layer of variable thickness is required across the entire margin in order to fit the most extensive crustal diving-ray phase observed on all the record sections at offsets exceeding 10–15 km.

4. The structure of the lower crustal layer is constrained between 60 and 140 km (Figure 7). It is lens shaped, with a maximum thickness of ~8 km between 85 and 140 km, thinning to ~2 km thickness at either end. The high velocities (7.2–7.5 $km\,s^{-1}$) are required to fit the travel time curves of the Moho reflections and of diving rays traveling through the upper part of the lens and recorded at offsets of 40–60 km on DOBH11, 50–60 km on DOBH12, 60–65 km on DOBH14, and 60–70 km on DOBH15. The average velocity gradient required to fit the diving rays within the upper part of the layer is 0.015 s^{-1}, and this velocity gradient is assumed to continue unchanged down to the Moho.

5. The Moho over the central portion of the profile is the interface separating the lower crustal velocities of 7.4–7.5 $km\,s^{-1}$ from upper mantle velocities of 7.9 $km\,s^{-1}$. In common with other refraction profiles on the North Atlantic margins, which define mantle velocities of 7.9–8.0 $km\,s^{-1}$, we find a relatively low upper mantle velocity of 7.9 $km\,s^{-1}$. The Moho dips with a gradient of about 7% to the SE, deepening from 14 km to 20 km over the region where it is constrained (i.e., between 60 and 140 km model space).

Resolution and Uncertainty

Zelt and Smith's [1992] inversion method provides a quantitative estimate of the resolution of the parameters used to specify the velocity model, based on the

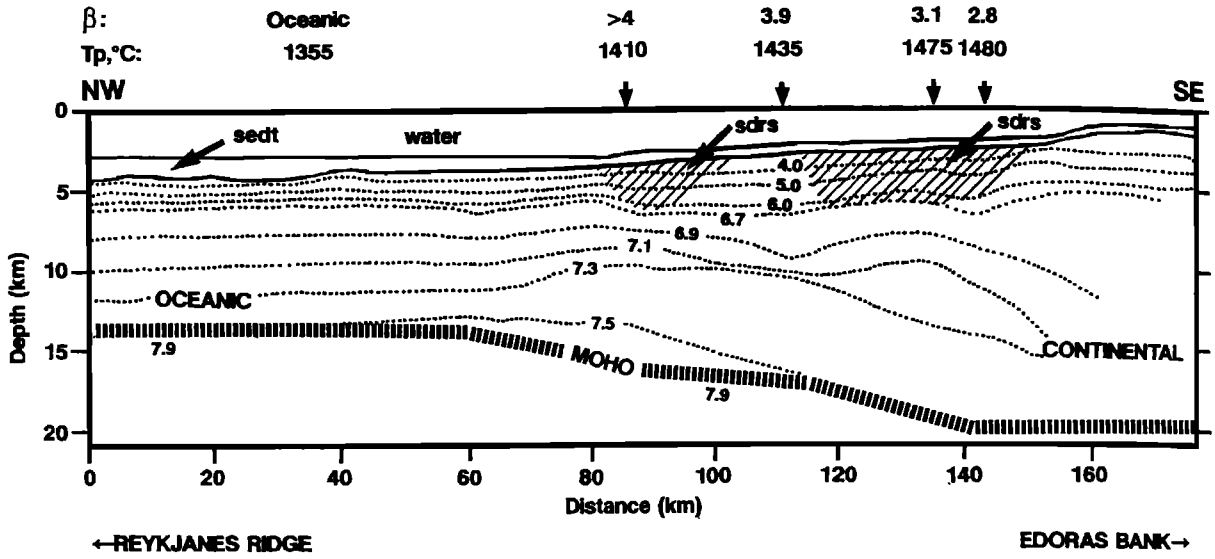

Figure 8. Final velocity model for Cam77. P wave velocities are contoured in kilometers per second, and cross-hatched areas denote where seaward dipping reflectors are imaged by the normal-incidence data. Stretching factor β and mantle potential temperature T_p at the time of continental breakup are shown along the top (see text for discussion).

relative number of rays that sample that parameter. A contoured plot of the resolution values for the final model (Figure 9) shows that the central area of the model, where there is good ray coverage is well-resolved. The low resolution values toward each end of the model reflect the reduced ray density, and in these areas the crustal structure is only poorly constrained. In general, the midcrustal regions where there are multiple crossing rays are resolved better than the uppermost and lowermost crust.

An estimate of the spatial uncertainty in the position of a specific interface node is obtained by perturbing the value of the node and observing the deviation in the travel time fit compared to that obtained for the unperturbed model. The perturbation is increased until the final model so obtained fits the observed data less well than the original model according to (1) the ability to trace rays to all observations; and (2) the result of an F test comparing the normalised misfit parameter χ^2 of the unperturbed and perturbed models. The maximum perturbation of the parameter (in both positive and negative directions) that allows a comparable fit to the observed data is a measure of its absolute uncertainty [*Zelt and Smith*, 1992]. The nodes of the interface separating the upper and midcrustal layer could be perturbed individually by, on average, ±0.24 km, or about ±4% of the interface depth without significantly degrading the travel time fit. The depth to the upper boundary of the high-velocity lower crustal layer appears poorly constrained, with an average uncertainty of about ±17% of the depth, a consequence of it being sampled by diving rays which traverse large parts

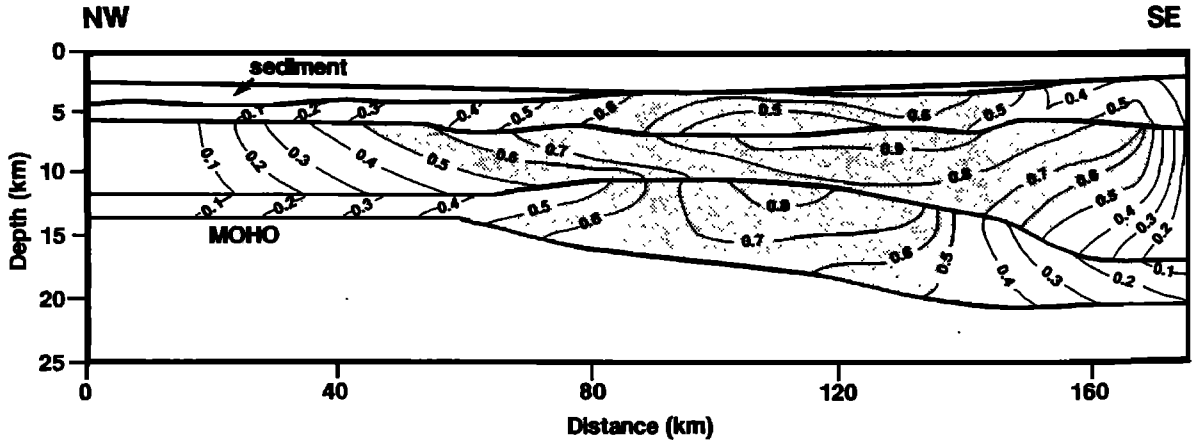

Figure 9. Contoured plot of the resolution values for the crustal velocity model for Cam77. Values greater than 0.5 indicate areas of the model that are reliable and well-resolved [*Zelt and Smith*, 1992].

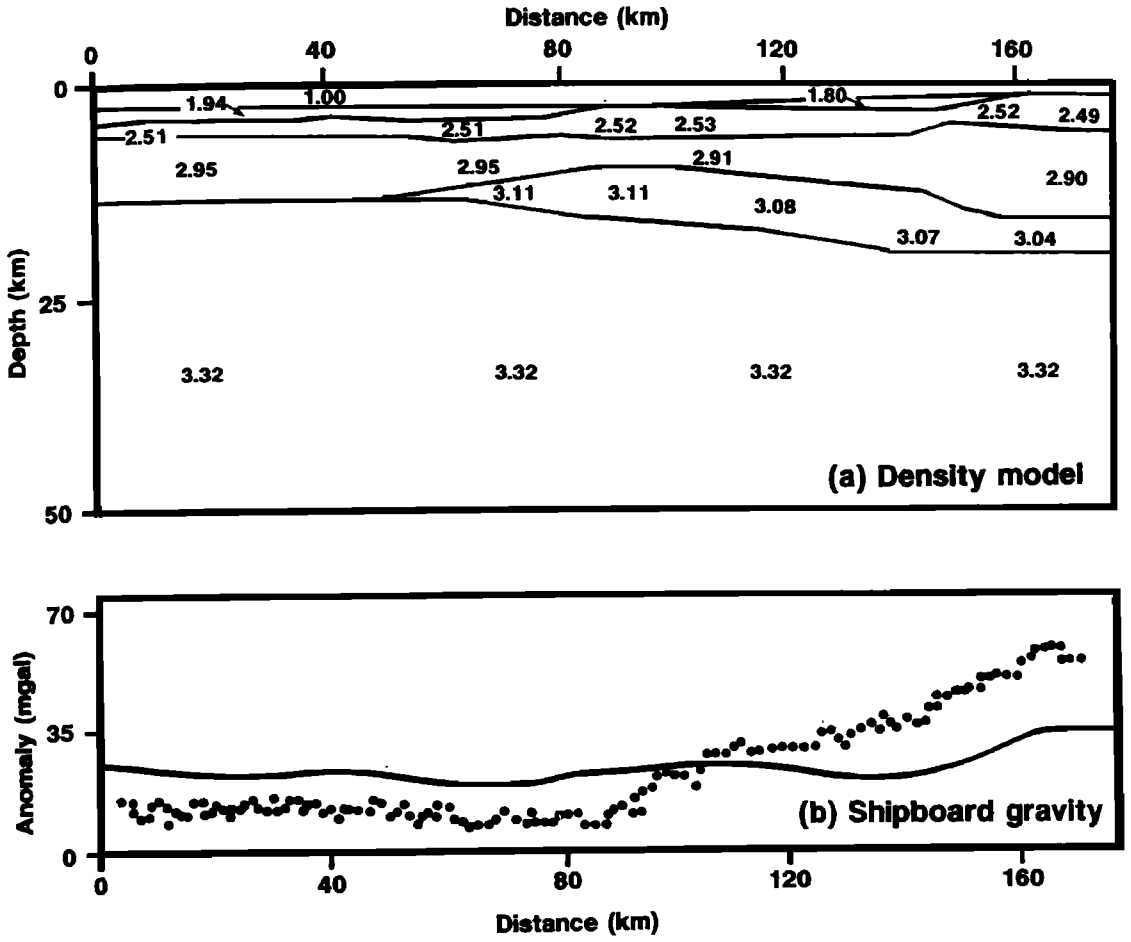

Figure 10. Initial gravity model for the Edoras Bank margin along the dip profile Cam77. Densities are calculated from the seismic velocities using a polynomial approximation to the mean velocity–density relationship of *Nafe and Drake* [1957]. (a) density model, numbers showing densities in units of 10^3 kg m^{-3}; (b) calculated free-air anomaly (solid line) plotted with shipboard observations (dots).

of the model along their path from source to receiver. The associated uncertainty is reduced to ±5–6% when the entire interface is perturbed rather than the individual nodes. The uncertainty on the Moho depth over the central portion of the model is, on average, ±1.6 km for individual node perturbation.

A similar method is used to estimate the uncertainty in the velocities. For the upper, middle, and lower crustal layers the average maximum perturbations to the velocities without significantly degrading the travel time fits is ±0.09, ±0.11, and ±0.18 km s^{-1} respectively, assuming a constant vertical velocity gradient within each layer.

Gravity Modeling

The aim of the gravity modeling was to establish whether the seismic velocity model generated from the wide-angle data is consistent with the available gravity data. A crustal density model was first prepared by assigning a density to each of the seismic velocities specified in the final model for Cam77 using a polynomial fit through the mid-points of the velocity-density data published by *Nafe and Drake* [1957]. This gives a poor fit to the observed gravity data (Figure 10), though this is unsurprising given the large scatter, and the variety of rock types in *Nafe and Drake*'s [1957] data. A better fit (Figure 11) is obtained by modifying the velocity-density relationship using values compiled for oceanic crust by *Carlson and Herrick* [1990].

A good fit between the observed shipboard and Seasat gravity data and the calculated free-air anomaly is obtained by varying the densities in the model by, at most, 100 kg m^{-3} from those calculated from the seismic velocities using the *Carlson and Herrick* [1990] relationship and by altering interface depths only in areas not constrained by seismic travel time modeling. The fit of the model free-air anomaly to the observed data is to within ±2 MGal, except toward the top of Edoras Bank where the misfit reaches 4 MGal on the Seasat data and a maximum of 8 MGal on the shipboard data (Figure 11).

The high-velocity lower crust in the velocity model corresponds to a body with density 3080 kg m^{-3} in

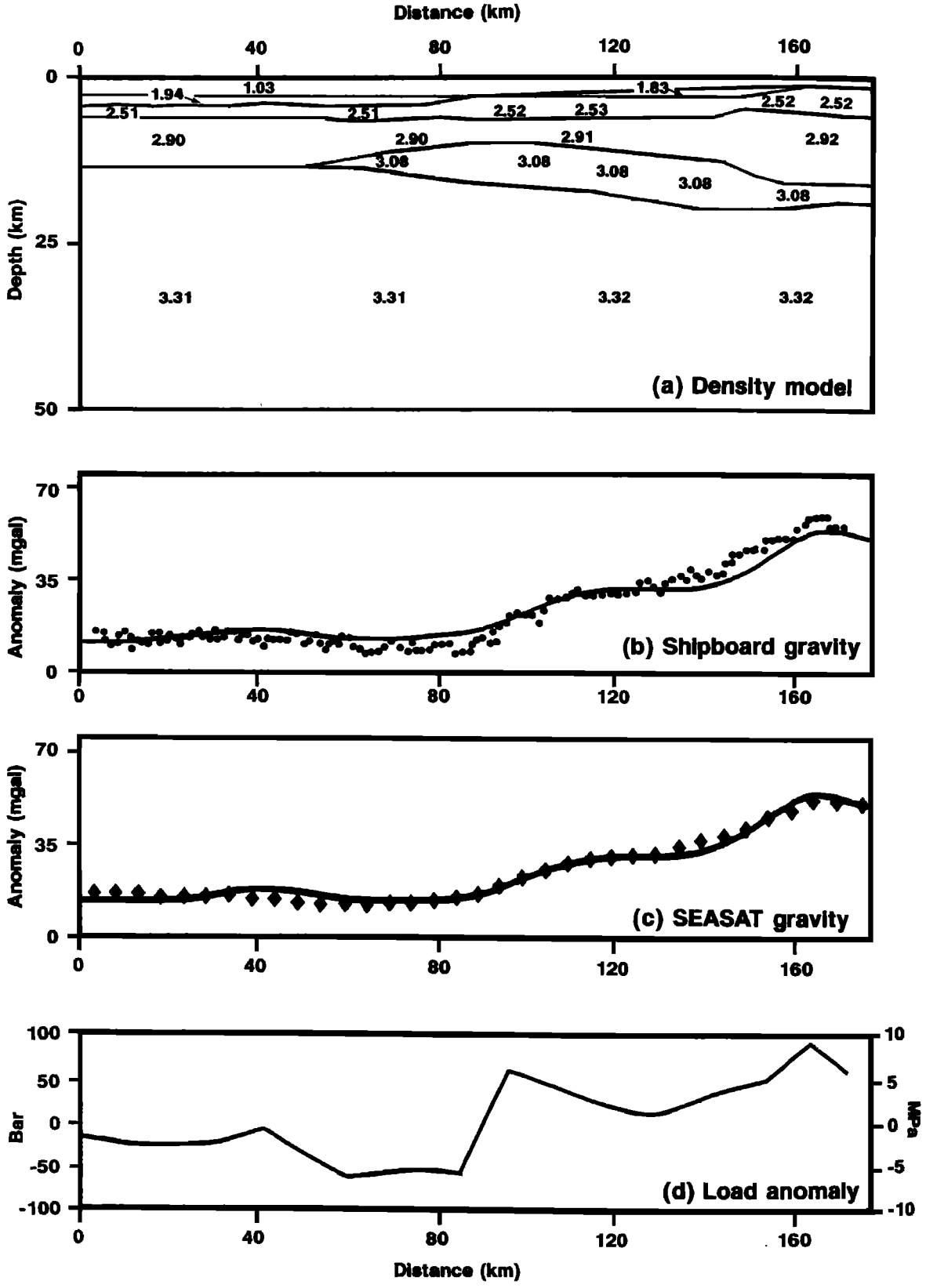

Figure 11. Final gravity model for the Edoras Bank margin along the dip profile Cam77. (a) density model, numbers showing densities in units of 10^3 kg m^{-3}; (b) calculated free-air anomaly (solid line) plotted with shipboard observations (dots); (c) calculated free-air anomaly (solid line) plotted with the Seasat gravity measurements (diamonds); (d) load anomaly along the profile.

the gravity model. A similar high-density lower crustal prism is required to fit the gravity data from the Hatton Bank margin 200 km to the northeast [*Prescott*, 1988]. The gravity modeling suggests that the body wedges out oceanward in a region poorly constrained by the travel time modeling. In order to fit the long-wavelength gravity variation across the continental margin, a decrease of 100 kg m^{-3} is required in the mantle density beneath the lower half of the continental margin and the adjacent oceanic crust (compare Figures 10 and 11). This mantle density is assumed to apply down to the base of the model at a depth of 50 km. Such a mantle density decrease is consistent with that expected due to depletion of the upper mantle by melt extraction [*Oxburgh and Parmentier*, 1977; *White and McKenzie*, 1989], with the bulk of the melt being extracted from the mantle between 50 km and the base of the overlying lithosphere [*White and McKenzie*, 1995]. Again, a similar decrease in mantle density over a similar depth range beneath the Hatton Bank margin to the northeast was required by *Prescott* [1988] to model the gravity there. The crustal model developed for the Edoras Bank continental margin is thus consistent with both seismic data and with gravity data for the region: in particular, a high-velocity, high-density body is required in the lower crust beneath the margin, and the underlying mantle density decreases across the margin from the continental to the oceanic ends.

Geological Interpretation

Continental Crustal Structure

The velocity structure beneath Edoras Bank is well-constrained only to depths of 5–6 km. The upper crustal velocity structure is similar to that determined in previous studies of the continental shelf west of Britain [e.g., *Scrutton*, 1972; *Jones et al.*, 1984; *Powell*, 1986; *Fowler et al.*, 1989]. Relatively low uppermost crustal velocities have also been observed elsewhere and may be caused by consolidated sediments or by weathering and fracturing of the basement material [e.g., *Jones et al.*, 1984].

The Continent-Ocean Transition

Shallow structure. The shallow structure of the continent-ocean transition consists largely of seaward dipping reflector sequences extending through the uppermost 4 km of crust across a zone some 70 km wide. Although early explanations suggested that sdrs may represent the prograding clinoforms of deltaic sequences, a volcanic origin for them was confirmed when sdrs were drilled successfully on DSDP Leg 81 and ODP Legs 104, 152, and 163 in the North Atlantic. Leg 81 drilled the top of the sdr sequence at two locations on the Edoras Bank margin (Figure 2) and found tholeiitic basalt lava flows that had been extruded under subaerial or very shallow marine conditions. The reflectors imaged on multichannel seismic profiles are likely to arise from impedance contrasts between the cores of basalt flows and their weathered tops, or interbedded volcaniclastic sediments, forming a complex interference pattern between the closely spaced flows [*Planke and Eldholm*, 1994].

Models for the formation of sdrs ascribe their shape to lava extrusion from an oceanward source with the seaward dip being caused by subsidence after extrusion in a manner akin to that observed and modeled for Icelandic lava flows [*Pálmason*, 1980]. The extrusion of lavas in the neovolcanic zones of Iceland through central volcanoes and the intersecting sets of fissure systems may provide a good analogue for volcanism on the highly stretched continental margin in the later stages of continental breakup [*Barton and White*, 1997]. Some authors suggest that the sdrs were extruded over oceanic crust as "sub-aerial seafloor spreading" [*Mutter et al.*, 1988], while others maintain that they were emplaced over thinned continental crust [e.g., *Hinz*, 1981; *Roberts et al.*, 1984].

The sheet-like, two-dimensional nature of the sdrs on Edoras Bank suggests that the basalt was extruded from fissures aligned parallel to the line of breakup [*Barton and White*, 1997]. Lead isotope studies of DSDP Leg 81 basalts from the margin suggest that they were erupted through Precambrian Rockall continental crust [*Morton and Taylor*, 1987]. Gravity and subsidence modeling disussed below also suggests that the sdrs of the Rockall margin are underlain by stretched continental material, evidence which supports *Hinz*'s [1981] model of sdr formation.

Deep structure. A striking feature of the the continent-ocean transition zone at Edoras Bank is the lens of high-velocity and high-density material which constitutes the lower part of the crust beneath the region of sdrs. The lens is ~90 km wide and reaches a maximum thickness of 8 km. The high-velocity lower crust of the Edoras Bank margin is not typical either of normal oceanic crust or of continental crust beneath the adjacent NW European mainland. Velocities in the lower crust of 7.2–7.6 kms^{-1} have been observed on other North Atlantic rifted margins, including the Hatton Bank margin [*Fowler et al.*, 1989; *Morgan et al.*, 1989]; the Vøring Plateau margin [*Mutter et al.*, 1988]; the East Greenland margin [*Mutter and Zehnder*, 1988]; the Møre margin [*Olafsson et al.*, 1992]; and the East Coast of the United States [*LASE Study Group*, 1986; *Holbrook et al.*, 1994; *Kelemen and Holbrook*, 1995].

The high-velocity material may represent crustal underplating [*Cox*, 1980; *Furlong and Fountain*, 1986] or intrusion of the preexisting crust [e.g., *Fowler et al.*, 1989] by partial melt generated from upwelling asthenospheric mantle [*White et al.*, 1987]. The observed seismic velocities in the lower crust on the Edoras Bank margin are consistent with those expected from partially fractionated and frozen melts derived from partial melting of anomalously hot asthenospheric mantle and suggest that the high velocities result from high MgO contents of the rock [*White and McKenzie*, 1989; *Kelemen and Holbrook*, 1995].

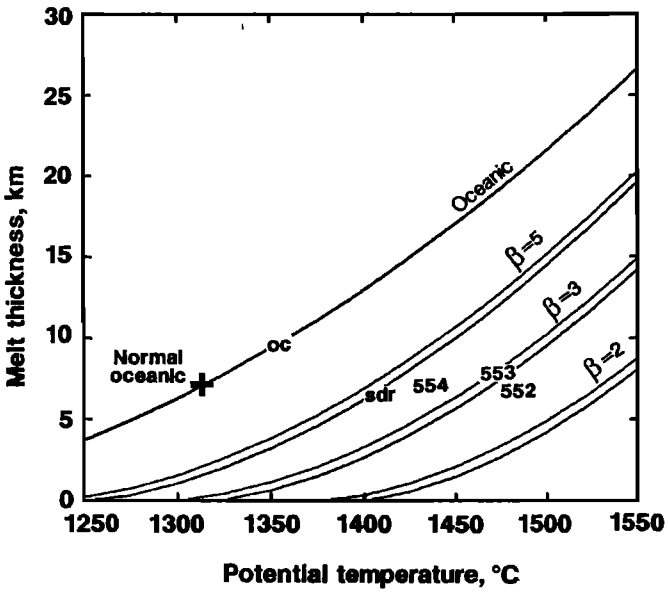

Figure 12. Thickness of melt generated by passive isentropic mantle decompression beneath lithosphere thinned by beta factors of 2, 3, and 5 by pure shear. For each stretching factor the upper and lower curves are for rift durations of 1 m.y. and 3 m.y., respectively. The curve labeled "oceanic" is the melt thickness generated beneath an oceanic spreading center where the mantle is allowed to decompress to the base of the igneous crust. Calculations follow *Bown and White* [1995a] in allowing compaction of the source mantle as melt is extracted, and use a value of 400 J kg^{-1} $°C^{-1}$ for the entropy change on melting. Cross labeled "normal oceanic" shows the mantle temperature required to produce a normal oceanic crustal thickness of 7 km [*White and McKenzie*, 1995]. Labels 552, 553, 554, and sdr show the mantle temperatures required to model the observed igneous thicknesses and stretching factors beneath ODP sites 552–554 and the lower set of seaward dipping reflectors, and "oc" shows the melt thickness and temperature of the oldest oceanic crust adjacent to Edoras Bank. Note how the mantle temperature decreases from the least stretched, most continentward site 552 to the youngest, most stretched oceanward site "oc".

Oceanic Crustal Structure

The most oceanward velocity structure constrained by travel time modeling is about 60 km from the NW end of Cam77 in 51 Ma crust. The crustal thickness of 9.7±1.5 km is ~3 km thicker than normal oceanic crust [*White et al.*, 1992]. This lies within the spread of values found elsewhere in the plume-influenced North Atlantic and suggests that a significant thermal anomaly associated with the Iceland plume extended at least as far as Edoras Bank at anomaly 23 time [*White*, 1992]. If the oceanic crust is generated entirely by passive upwelling beneath the spreading center, an asthenospheric potential temperature of ~1355°C, about 50°C hotter than normal, is required to produce the 9.7 km of oceanic crust observed (Figure 12) [*Bown and White*, 1994].

Subsidence of the Edoras Bank Margin

The water-loaded subsidence history of the DSDP holes 552 and 553, which lie over the upper set of sdrs, and of hole 554, on the block between the two sets of sdrs termed the "outer high" by *Roberts et al.* [1984] (Figure 2) was calculated by backstripping the sediments and using the paleowater depths reported by *Murray* [1984]. All the holes bottomed in extrusive lava flows of early Eocene age deposited at or near sea level, providing good depth control at the time of breakup. Paleowater depths are more uncertain over the middle Tertiary because the paleontological control is less good in the increased water depths (Figure 13).

We model the subsidence assuming a finite duration rifting episode lasting from 58–56 Ma, with allowance for melt generation as the underlying mantle wells up and decompresses. The melting and subsidence model is described by *Bown and White* [1995a,b]. We assume bulk pure shear and dry mantle melting. The thermal evolution and melt generation are derived in two stages. First, we calculate the temperatures ignoring the thermal consequences of melting but with allowance for heat loss during finite duration rifting. Second, we correct these temperatures for the absorption of latent heat by the melting process and allow for the effect of mantle compaction due to the extraction of melt.

The subsidence is calculated assuming that local isostatic equilibrium is maintained and is dependent on three main factors. First, crustal thinning as rifting proceeds causes subsidence, while the thickening of the crust as melt is added to it acts to oppose this and may even cause uplift. Second, the reduced density of a layer of underlying anomalously hot asthenosphere causes uplift. Third, in the postrift phase, subsidence occurs if the asthenosphere temperature decreases, and as the lithosphere cools and thickens.

Note that these theoretical calculations assume that all the melt is accumulated in the crust directly above the mantle source region without lateral flow and that all the melt results from passive mantle decompression beneath the rift with no additional melt produced by active circulation in the underlying mantle. As we discuss later, both these assumptions are likely to be untrue in detail but do provide reasonable approximations for the modeling. The absolute mantle temperatures we infer are dependent on the values of many constants in the calculations, all of which have associated uncertainties. However, the relative temperature differences derived from our modeling are constrained better, with uncertainties of the order of only 10–20°C.

For each of the subsidence curves we model there are several constraints. These are the basement subsidence history, derived from backstripping the sediments; the amount of melt added to the crust; and the stretching factor β. The last two are derived from the seismic results. As Figure 12 demonstrates, the melt thickness and β allow us to deduce the mantle temperature at the time of rifting, while the postrift subsidence gives information on the mantle cooling history. In the case of Edoras Bank, there is a rapid subsidence phase shortly

after breakup which is particularly striking in data from DSDP 553 (Figure 13b). We model this by allowing the asthenospheric mantle temperature anomaly to decay back to normal by ~50 Ma.

The total melt thickness is calculated from the seismic results, assuming that the whole of the sdr sequence and 50% of the high-velocity lower crust represents synrift igneous rock added to the crust. The remaining thickness represents stretched residual continental crust, from which we can calculate a stretching factor β if we know the initial crustal thickness. We use an initial continental crustal thickness of 30 km, assuming that an earlier phase of Mesozoic stretching reduced the thickness from its normal value of 32 km beneath Britian [*White et al.*, 1987]. The Mesozoic stretching affected the entire NW European margin creating, inter alia, the Rockall Trough and Hatton-Rockall Basin.

Although the percentage of intruded igneous rocks in the lower crust is unknown, it makes little difference to the inferred mantle temperatures and subsidence curves because, if the thickness ascribed to igneous rock is increased, then the inferred β value is also increased, and the net result of this is that the inferred mantle temperature required to produce the increased melt thickness is little changed (Figure 12). For example, if we consider the region mid-way down the margin between the two sets of sdrs, the final nonsedimentary crustal thickness is 14 km, of which the lowermost 6.5 km exhibits seismic velocities greater than 7.3 km s^{-1} and is therefore intruded or underplated. Assuming no igneous addition to the upper crust, we find a total igneous thickness of 3.2 km and a β of 2.8 if the high-velocity wedge is 50% intruded, or an igneous thickness of 6.5 km and a β of 4.0 if it is 100% intruded. For stretching over a 2 m.y. period these two cases require mantle potential temperatures of 1420°C and 1425°C, respectively. Indeed, if there were no residual continental crust at all, and the crust here was fully oceanic, the 14 km thickness would require a mantle temperature of 1415°C (Figure 12). These mantle temperature estimates are so similar as to be indistinguishable and are therefore robust determinations of the temperature, despite our lack of knowledge of the percentage of igneous intrusion in the crust.

The theoretical subsidence curves which best fit the observed basement subsidence and melt thicknesses (solid lines on Figure 13) predict that when rifting started at 58 Ma, there was an initial small subsidence until the continuing extension allowed mantle decompression to

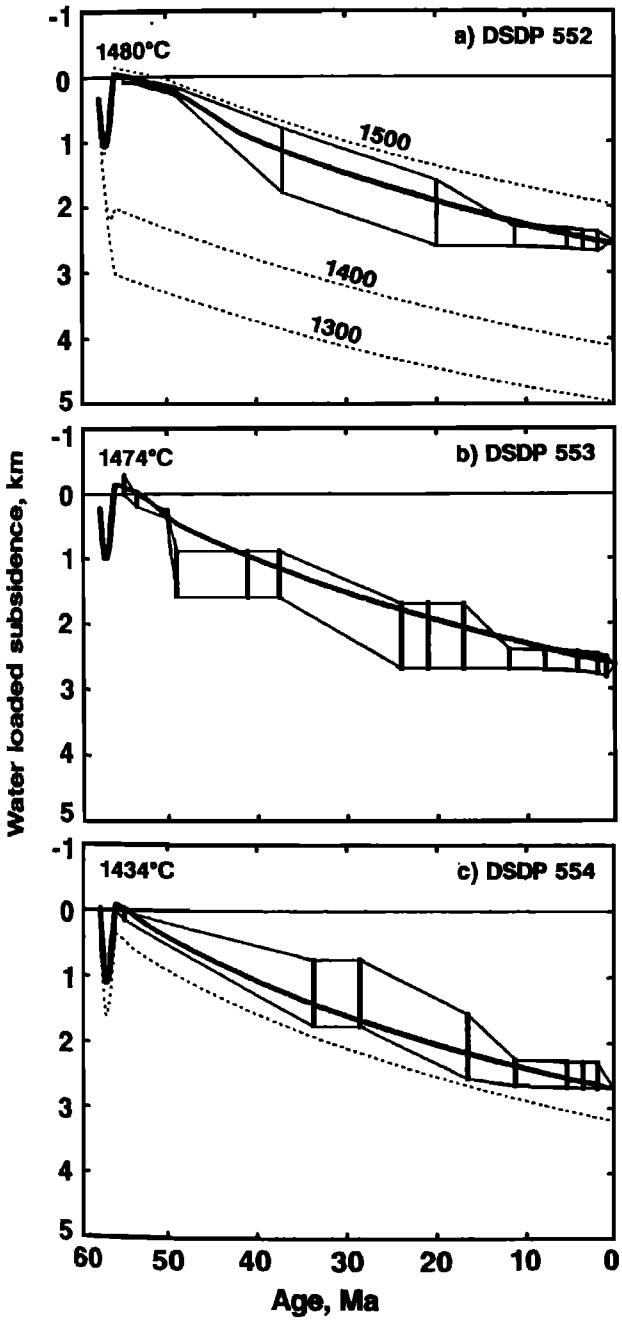

Figure 13. Water-loaded subsidence curves from DSDP holes on the Edoras Bank continental margin (see Figure 2 for location). Vertical bars show basement depths deduced from sediment cores using *Cande and Kent*'s [1992] timescale and *Murray*'s [1984] estimates of paleowater depths. The stretching factor β at each site is calculated from the crustal thickness. Solid lines show best fitting subsidence curves calculated from a finite duration rifting episode between 58 and 56 Ma, with allowance for melt generation [*Bown and White*, 1995a]. The asthenospheric mantle potential temperature at the time of breakup is annotated on each curve: this decays back to a normal mantle potential temperature of 1300°C by ~50 Ma. (a) Hole 552, at the landward end of the profile, with an initial water depth prior to stretching of 500 m: dashed lines show theoretical subsidence curves that would result from mantle temperatures of 1300, 1400, and 1500°C. (b) Hole 553, over the upper set of sdrs, with an initial water depth prior to stretching of 500 m. (c) Hole 554, over the "outer high" lying between the two sets of sdrs (Figure 2): best fitting solid line requires the top of the crust prior to stretching to lie at sea level: dotted line shows theoretical subsidence curve with an initial 500 m water depth.

generate significant quantities of melt. This was then frozen in the crust, thickening it and causing uplift to sea level as isostatic balance was maintained. The inferred synrift igneous thickness in the crust beneath the upper sdrs (Holes 552 and 553) is generated from mantle at a temperature of 1475–1480°C, stretched by β factors of 2.8–3.1 (Figures 13a and 13b).

In order to account for both the igneous thickness and the final subsidence at Holes 552 and 553 the top of the crust had to be about 500 m below sea level prior to the rifting at 58 Ma. This is consistent with the earlier phase of Mesozoic stretching mentioned above.

Subsidence at Hole 554 was modeled in a similar way (Figure 13c), requiring a somewhat greater β factor of 3.9, consistent with its more oceanward location (Figure 2), and a rather lower synrift mantle temperature of 1435°C. Farther oceanward still, the igneous thickness and final subsidence of the lower set of sdrs require a stretching factor in excess of 4.0 and a further decreased mantle temperature of 1410°C. However, the striking difference between the subsidence at these two oceanward locations compared to that of the upper set of sdrs is that the prerift depth must have been close to sea level: if the same 500 m pre-rift depth is assumed as for the upper sdrs then the resultant subsidence curve (dotted line, Figure 13c), is too deep to match the observations.

The subsidence history at different locations across the margin shows a consistent pattern of increasing β factors in an oceanward direction (Figure 7) coupled with decreasing synrift mantle temperatures from 1480°C at the most landward site (hole 552) through 1410°C over the lower set of sdrs, to 1355°C at the time of anomaly 23 when fully oceanic crust was being generated (Figure 12). This is consistent with a decrease in mantle temperature as rifting proceeded, since the most oceanward sites are the youngest. The relatively rapid decrease in mantle temperature is also in agreement with the subsidence history at individual DSDP sites: our models require the layer of abnormally hot asthenospheric mantle to have been, at most, only a few tens of kilometers thick, and that the thermal anomaly decayed over a period of only ~10 m.y. (e.g., Figure 13b). This is consistent with the rapid asthenospheric mantle temperature decrease, because a very thick layer of abnormally hot mantle could not have lost its heat conductively in the short time period we find, but a thin layer of mantle could have rapidly been absorbed in decompression melting beneath the developing rift.

The region between the two sets of sdrs, sometimes called the outer high, may be either a block of heavily intruded continental crust or, by analogy with a similar feature reported from the Hatton Bank margin to the north, it may be a late stage igneous intrusion that

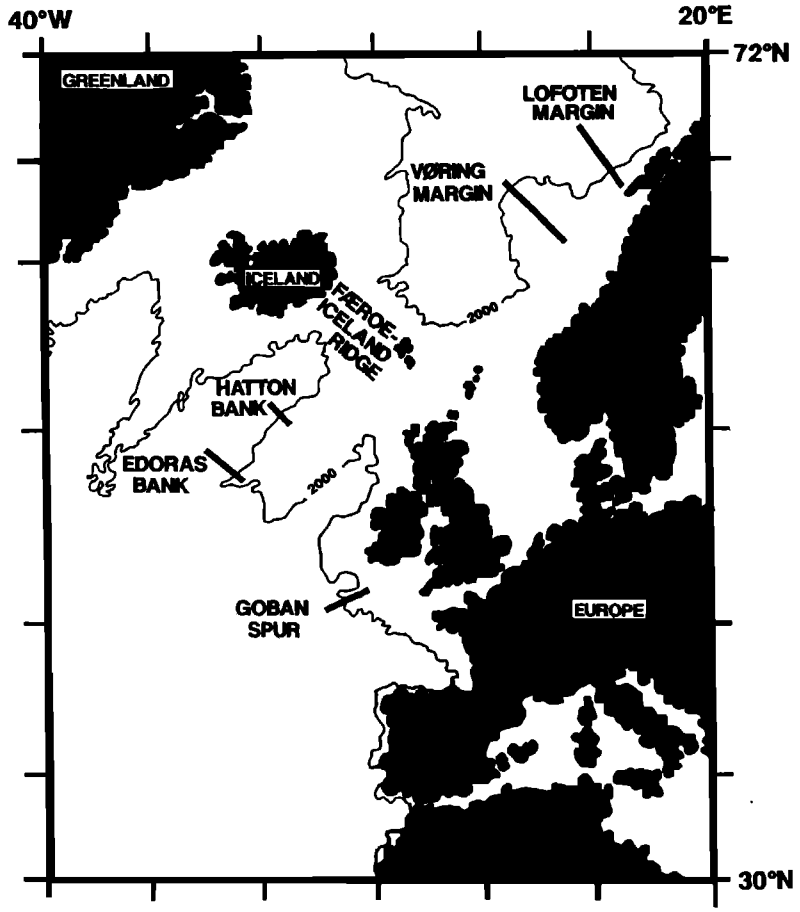

Figure 14. Locations of crustal transects shown in Figure 15, along the NW margin of Europe. Simplified bathymetry is shown contoured in meters.

has obliterated any preexisting seismic layering [*White et al.*, 1987; *Morgan et al.*, 1989], or it may represent a central volcano cut by fissures that was a focus of melt extrusion in a manner similar to that observed in the neovolcanic rift zones of Iceland [*Barton and White*, 1997]. In the Edoras Bank region the outer high forms a block at least 18 km wide by 50 km long, but it passes laterally along strike into a region of normal upper crustal layering identical to that caused by extrusive basalt flows [*Barton and White*, 1997]. Our subsidence modeling suggests that the prerift basement was about 500 m deeper to the east of the outer high. We consider the most likely interpretation of the outer high in the Edoras Bank region to be that it represents a coherent block of continental crust, probably bounded by faults which allowed the formation of small basins around it during the earlier phase of Mesozoic rifting that affected the entire NW European margin. However, as the Tertiary rifting proceeded this block must have become heavily intruded and covered by the lava flows penetrated by DSDP Hole 554. The eventual location of continental breakup lay to its west.

Lateral Extent and Temperature of the Mantle Plume

Excess melt thicknesses as extruded sdrs and intruded high-velocity lower crustal prisms are found along the entire NW European margin from the Lofoten margin off Norway in the north to the Edoras Bank margin in the south (Figures 14 and 15). This is in marked contrast to the structure of margins formed away from the influence of mantle plumes, such as that of the Goban Spur (Figure 15e). For each well-determined crustal section we use the inferred igneous thickness and stretching factor to deduce the mantle potential temperature at the time of rifting (Table 1). For sections over thinned continental crust we use a duration of 2 m.y. for the stretching phase (Figure 12) and assume that the mantle wells up passively in response to the lithospheric thinning.

It is striking that the inferred mantle temperatures at the time of continental breakup were about 200°C above normal (1500±50°C) along a 2000 km long stretch of the NW European margin, dropping off only at the distal ends (solid line, Figure 16). However, as rifting developed into fully fledged seafloor spreading, the inferred mantle temperatures away from the center of the plume decreased rapidly (dashed line, Figure 16). Far from the plume center, such as off Edoras Bank, the mantle temperatures during the early stages of seafloor spreading were only ~50°C above normal but still remained high (~200°C above normal) in the central region where the Færoe-Iceland Ridge was being formed directly above the core of the plume. The temperature distribution developed once full seafloor spreading was underway is similar to that found at present along a transect running from Iceland along the spreading center of the Reykjanes Ridge [*White et al.*, 1995].

The mantle temperature decrease that accompanied continental breakup can be seen clearly on dip sections across the margin at those locations where there are sufficient measurements of the crustal thickness to construct transects (i.e., Lofoten, Vøring, Hatton Bank, and Edoras Bank margins, Figure 17). Inferred temperatures decreased by 100–150°C between the time of emplacement of the thickest igneous sections on the margin and the time of formation of the adjacent oceanic crust.

In summary, the temperature beneath the northern North Atlantic at the time of continental breakup was anomalously high everywhere over a 2000 km long region and was close to 1500°C: this is a similar temperature to that inferred from geochemical data for the production of flood basalts elsewhere in the world [*White and McKenzie*, 1995]. As rifting proceeded, the temperature dropped rapidly and attained a distribution similar to that found at the present day around Iceland: the present-day temperatures can be explained by a relatively narrow (~100–200 km diameter) rising core of hot mantle in the plume, with a large surrounding region of rather cooler asthenospheric mantle surrounding the core and extending distances of more than 1000 km from the center [*White et al.*, 1995].

There are striking similarities in the pattern of igneous accretion along the northern North Atlantic margins described here to that found off the East Coast margin of the United States. On the U.S. margin, sdrs have been found lying above lower crust exhibiting high velocities of 7.2–7.5 kms^{-1}, indicative of underplating or igneous intrusion. The igneous section reaches a 25 km thickness on the continental margin, decreasing rapidly offshore to ~8 km thick oceanic crust. The thick igneous section forms a long, narrow band extending more than 1000 km along the U.S. East Coast, with a width of 60–80 km [*LASE Study Group*, 1986; *Tréhu et al.*, 1989; *Sheridan et al.*, 1993; *Holbrook et al.*, 1994; *Kelemen and Holbrook*, 1995]. As with the northern North Atlantic, the large igneous thickness, the sdrs, and the high-velocity lower crust on the continental margin are indicative of high mantle temperatures at the time of continental breakup, reaching about 1500°C above normal. The decrease in igneous thickness to ~8 km in the adjacent oceanic crust suggests a rapid decrease in mantle temperature over a period of ~5 m.y., although the thicker than normal oceanic crust shows that the postbreakup mantle temperature remained higher than normal. All these features mirror those we find on the northern North Atlantic margins.

How can this melt and inferred temperature distribution in the northern North Atlantic be explained? One possibility is that there was active convection in the mantle beneath the margin which fed melt into the crust over a period of several million years of rifting prior to continental breakup. If this were the case, then the mantle temperatures could have been lower than calculated from Figure 12, which assumes a single stage of passive decompression melting. They could not, however, decrease to as low as the 1355°C which is inferred for the oldest oceanic crust adjacent to Edoras Bank,

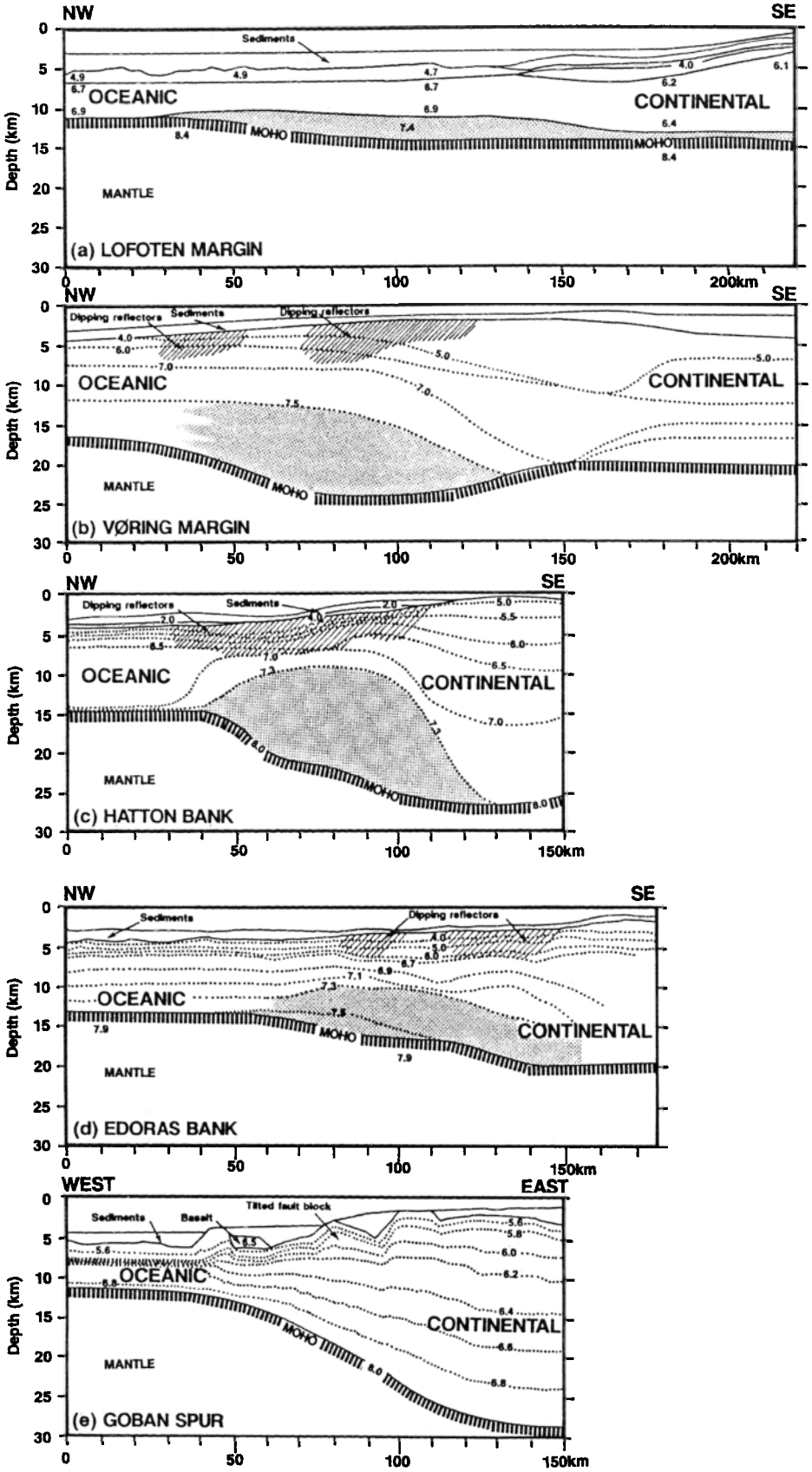

Figure 15. Crustal transects for areas of the NW European margin (see Figure 14 for location) developed using principally wide-angle seismic data. In each case, P wave velocities are contoured in kilometers per second. Cross-hatching denotes areas where extrusive basaltic sequences (sdrs) are imaged. Stippled regions are high-velocity lower-crustal bodies interpreted as intruded or underplated igneous rock. (a) The Lofoten Basin margin [*Goldschmidt-Rokita et al.*, 1994]; (b) the Vøring Plateau margin [*Mutter and Zehnder*, 1988]; (c) the Hatton Bank margin [*Fowler et al.*, 1989]; (d) the Edoras Bank margin (this study); and (e) the "nonvolcanic" Goban Spur margin by way of contrast to the "volcanic" margins to the north [*Horsefield et al.*, 1994].

Table 1. Summary of North Atlantic Data Discussed in the Text

Location	Data[a]	Reference	sdrs?	Latitude, °N	Longitude, °E	D[b], km	β	Melt, km	T_p[c], °C
			Oceanic						
Lofoten	OBS49	1	no	69.50	11.01	-1160		7.0	1312
Lofoten	OBS18	2	yes	69.08	9.62	-1085		10.1	1360
Lofoten	OBS27	3	no	69.45	8.71	-1080		7.3	1317
Lofoten	OBS28	3	no	69.29	9.03	-1080		8.7	1340
Lofoten	OBS46	1	yes	69.23	9.17	-1080		8.2	1332
Lofoten	OBS19	2	yes	68.86	8.89	-1050		11.3	1377
Lofoten	OBS44	1	no	69.03	7.97	-1030		9.3	1349
Lofoten	OBS20	2	yes	68.70	8.38	-1020		11.8	1384
Lofoten	OBS21	2	yes	68.52	7.86	-990		12.3	1391
Lofoten	OBS41	1	yes	68.74	6.36	-960		10.9	1372
NE Greenland	ESP19	4	no	74.44	-13.20	-930		7.0	1312
NE Greenland	ESP20	4	yes	73.71	-13.37	-930		7.4	1319
NE Greenland	ESP22	4	no	72.90	-16.82	-820		12.9	1399
Vøring	ESP13	4	no	68.51	3.10	-820		12.5	1394
Møre margin	ESP46	5	no	64.25	-0.43	-480		10.4	1365
Møre margin	ESP45	5	no	64.10	0.20	-480		11.7	1383
Færoe-Iceland Ridge	OBS43	6	no	63.86	-6.10	-180		9.8	1356
Færoe-Iceland Ridge	OBH	7	no	62.68	-9.11	0		30.0	1580
Færoe-Iceland Ridge	OBS[d]	6	no	62.44	-10.21	55		13.7	1409
Færoe-Iceland Ridge	OBS[d]	6	no	62.00	-11.47	90		11.8	1384
SE Greenland	82–01[e]	8	yes	65.46	-33.39	240		13.9	1412
Hatton Bank	OBS4	9	yes	59.63	-19.53	680		10.8	1370
Hatton Bank	ESPH	10	yes	59.43	-19.27	680		11.1	1374
Hatton Bank	ESPG	11	yes	59.36	-19.02	680		11.2	1376
Edoras Bank	OBH14	12	no	56.64	-24.07	1120		9.7	1354
			Continental						
Lofoten margin	OBS114	3	yes	69.14	9.43	-1080	4.5	3.0	1350
Lofoten margin	OBS210	3	no	68.96	9.62	-1080	3.8	1.3	1330
NE Greenland	ESP18	4	yes	75.10	-11.31	-1070	4.2	5.5	1399
Vøring margin	ESP12	4	yes	68.26	4.10	-820	2.6	9.6	1519
NE Greenland	ESP 23	4	yes	72.84	-17.97	-800	2.6	6.3	1475
Møre margin	ESP44	5	yes	63.92	0.96	-480	3.4	9.1	1480
Hatton Bank	ESPE	11	yes	59.17	-18.69	680	3.3	11.0	1502
Hatton Bank	ESPC	11	yes	59.04	-18.46	680	2.4	10.9	1545
Edoras Bank	Lower sdrs	12	yes	56.46	-23.83	1120	4.7	6.2	1410
Edoras Bank	554	12	no	56.29	-23.53	1120	3.9	6.5	1434
Edoras Bank	553	12	yes	56.09	-23.34	1120	3.1	7.0	1474
Edoras Bank	552	12	yes	56.04	-23.23	1120	2.8	6.3	1480

References: 1, *Kodaira et al.* [1995]; 2, *Mjelde at el.* [1992]; 3, *Goldschmidt-Rokita et al.* [1994]; 4, *Mutter and Zehnder* [1988]; 5, *Olafsson et al.* [1992]; 6, *Makris et al.* [1995]; 7, *Bott and Gunnarsson* [1980]; 8, *Larsen and Jakobsdóttir* [1988]; 9, *Morgan et al.* [1989]; 10, *Spence et al.* [1989]; 11, *Fowler et al.* [1989]; 12, this paper.

[a]Data type: ESP, two-ship expanding spread profile; OBS or OBH, ocean bottom seismograph or hydrophone; 81–20, 82–03, sonobuoys; Edoras Bank temperatures are derived by subsidence modeling over the lower sequence of sdrs and at DSDP boreholes 552, 553, and 554, using thicknesses along CAM77 from this paper.

[b]Distance from inferred center of the Iceland mantle plume, taken as the center of the Greenland-Iceland-Færoe Ridge. Negative values to the north of the plume center, positive values to the south.

[c]Potential temperature of asthenospheric mantle at the time of crustal generation (see Figure 10), assuming isentropic decompression of dry mantle, and using values from *Bown and White* [1994].

[d]We assume the crust here is oceanic, though *Makris et al.* [1995] assume it is continental.

[e]Moho depth is only poorly constrained from weak signals close to or at noise level at offsets of 15–30 km.

because at such a temperature dry mantle melting only starts to occur for β factors greater than 2.4 (Figure 12) (i.e., lithospheric lid thinner than 50 km). If this were the case, it would take far more than the few million years of rifting available to build up the large thicknesses of melt beneath the upper set of sdrs observed on the Edoras Bank margin, where β factors were only ~3.

An alternative explanation for enhanced melt thicknesses might be that melt flowed laterally along the rift from a central point: if this happened it would again mean that our inferred mantle temperatures along the

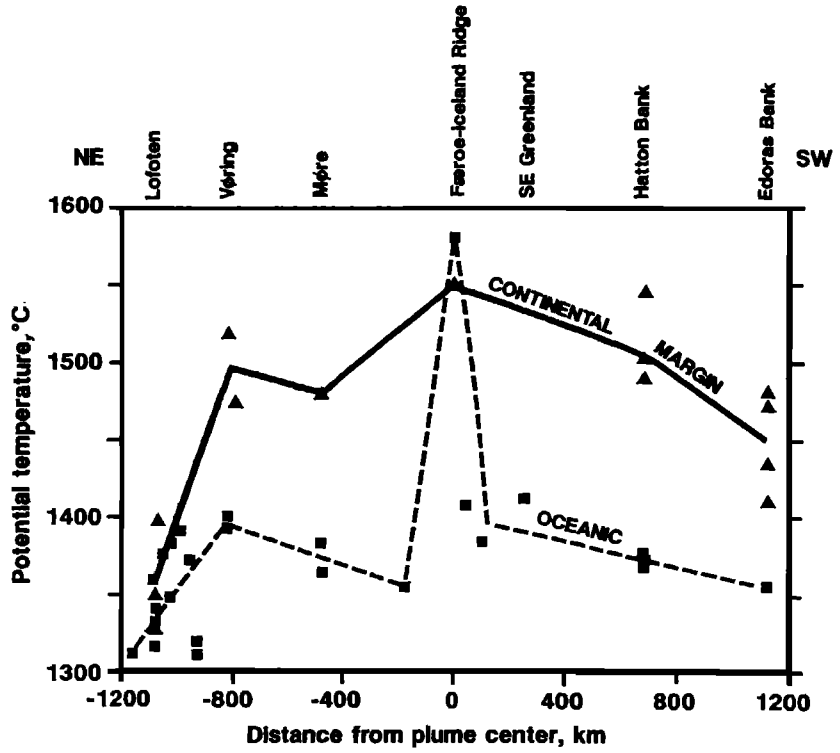

Figure 16. Variation in asthenospheric potential temperature along the North Atlantic margins during and immediately following continental breakup. Data sources are shown in Table 1. Temperatures were estimated using the method outlined in Figure 12, using a rift duration of 2 m.y. Distances are measured along strike from the shallowest part of the Færoe-Iceland Ridge for NW European margin locations and of the Greenland-Iceland Ridge for Greenland margin locations.

margin are overestimates. It is well documented that melt can flow many hundreds of kilometers in dykes through the lower continental crust: the Mackenzie dyke swarm in the Archean crust of Canada is one example [*LeCheminant and Heaman*, 1989]. However, it is less clear that melt will flow laterally over long distances through heavily rifted regions. In Iceland, for example, dykes are known to extend only a few tens of kilometers from central intrusion points [*Sigurdsson and Sparks*, 1978], without propagating along the adjacent Reykjanes Ridge spreading center. Dykes in the lower continental crust probably travel at a level of neutral buoyancy [*Lister and Kerr*, 1991], but it seems likely that the heavily faulted and thinned region along the continental rift would allow the melt to rise rapidly to the surface rather than traveling laterally more than 1000 km. We also note that the inferred igneous thickness does not decrease markedly with distance away from the central region of the mantle plume, as might be expected if the source of the bulk of the melt were in the center. We suggest therefore that there was no major long-distance lateral migration of melt along the zone of incipient breakup.

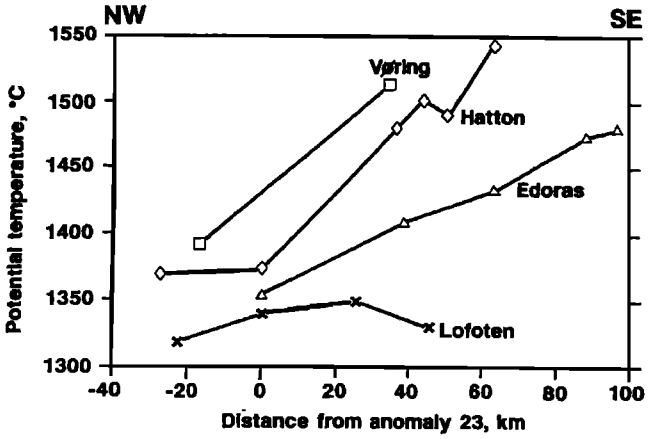

Figure 17. Asthenospheric potential temperature profiles across the NW European continental margin at the time of continental breakup. Distances are measured from the onset of magnetic anomaly 23 in each area. Positive distances denote locations landward (SE) of anomaly 23, while negative distances denote locations oceanward (NW) of anomaly 23.

The most probable explanation for the enhanced mantle temperatures at the time of rifting is that they were caused by the transient conditions associated with the initiation of a new plume [*Richards et al.*, 1989; *White and McKenzie*, 1989; *Campbell and Griffiths*, 1990]. However, the plume instability may not necessarily have generated a spherical rising head but may have taken the form of rising sheets of abnormally hot mantle [*White*, 1992; *White and McKenzie*, 1995]. It is not uncommon to find a triple junction geometry of instabil-

ities in convection experiments, where the three rising sheets near the base of the convecting layer tend to coalesce and to develop into a more axisymmetric-shaped plume as they rise toward the surface [*Houseman*, 1990]. This is an attractive model to explain the distribution of melt in the Tertiary Igneous Province of the North Atlantic emplaced during continental breakup. It is possible that two rising sheets extended north and south along the line of the succeeding North Atlantic opening, while a third sheet may have extended beneath Greenland to the Disko Island region on the west coast of Greenland, where there was voluminous high-temperature volcanism at the same time. The transient sheet-like anomalies may then have developed, as do the numerical models, into an approximately axisymmetric plume centered on the Færoe-Iceland Ridge, which has continued until the present day, and is now centered beneath eastern Iceland.

Whether or not the scenario described above is the correct explanation, it is clear that along most of the North Atlantic continental margins the transient thermal anomaly died away quickly (Figures 16 and 17) and that the layer of anomalously thick asthenospheric mantle was relatively thin, based on the evidence from the subsidence curves.

A similar scenario can be postulated for the U.S. East Coast margin. The thick igneous section and the high-velocity lower crust found there can be explained by enhanced mantle temperatures at breakup time. Although *Holbrook and Kelemen* [1993] have argued that the magmatism on the U.S. margin was not caused by a mantle plume on the grounds that the igneous thickness is constant along the margin and that there is a rapid decrease in thickness across the margin, it is clear that both these features are identical to those seen in the northern North Atlantic. Also, there was an undisputed mantle plume in the North Atlantic, which presently lies beneath Iceland. It is true that there is no obvious plume track off the U.S. margin similar to the Færoe-Iceland-Greenland track of the Iceland plume, but as *White and McKenzie* [1989] comment, it is likely that the plume responsible for the U.S. East Coast magmatism could have migrated shortly afterwards beneath North Africa: although it would not then have left a narrow track in the subsequently formed oceanic crust, the greater than normal thickness of the oceanic crust adjacent to the U.S. margin points to the presence of a nearby plume.

Conclusions

At Edoras Bank we find a thick intrusive and extrusive synrift igneous section on the rifted continental margin. This is similar to the evidence for an outburst of magmatism at other locations along the northern North Atlantic margins formed in the early Tertiary: despite its distal location, over 1000 km from the presumed center of the Iceland plume, the magmatic activity at Edoras Bank was similar in style and in volume to that at locations much closer to the center. This observation, together with evidence from the subsidence history of the margins, suggests that the asthenospheric mantle was abnormally hot, approximately 200°C above normal, beneath the entire northern North Atlantic margin at the time of continental breakup. We attribute this primarily to the transient conditions accompanying the initiation of a new mantle plume and suggest that it may have initially exhibited a triple-junction sheet-like shape, which subsequently developed into the axisymmetric shape found today beneath Iceland. The transient abnormally high temperatures died away quickly, over 10 m.y. or less, as the plume developed, with the highest temperature mantle found subsequently only in the narrow rising core of the plume which was responsible for generating the Færoe-Iceland-Greenland Ridge.

The line of continental breakup occurred along the edge of the region stretched and thinned during the earlier Mesozoic rifting events. As the margin broke up, it may have contained relatively coherent blocks of continental crust, possibly inherited from the earlier Mesozoic rifting, and similar to those found on nonvolcanic margins. However, the rapid intrusion of huge quantities of molten rock into the rifting margin destroyed the coherence of these blocks and, by weakening the crust, allowed a rapid and relatively narrow breakup zone in the transition from continental to oceanic crust.

Acknowledgments. A.J.B. was funded by the NERC and Schlumberger Cambridge Research. Seismic reflection data were processed by Simon Petroleum Technology Ltd. and in-house using Merlin SKS and PROMAX software. We thank Keith Louden and the Associate Editor for their helpful reviews. Department of Earth Sciences, Cambridge contribution 4709.

References

Barton, A. J., and R. S. White, Volcanism on the Rockall continental margin, *J. Geol. Soc. London*, in press, 1997.

Bott, M. H. P., and K. Gunnarsson, Crustal structure of the Iceland-Faeroe Ridge, *J. Geophys.*, *47*, 221–227, 1980.

Bown, J. W., and R. S. White, Variation with spreading rate of oceanic crustal thickness and geochemistry, *Earth Planet. Sci. Lett.*, *121*, 435–449, 1994.

Bown, J. W., and R. S. White, The effect of finite duration extension on melt generation at rifted continental margins, *J. Geophys. Res.*, *100*, 18,011–18,029, 1995a.

Bown, J. W., and R. S. White, Finite duration rifting, melting and subsidence at continental margins, in *Rifted Ocean-Continent Boundaries*, edited by E. Banda, M. Torné, and M. Talwani, pp. 31–54, Kluwer Acad., Norwell, Mass., 1995b.

Campbell, I. H., and R. W. Griffiths, Implications of mantle plume structure for the evolution of flood basalts, *Earth Planet. Sci. Lett.*, *99*, 79–93, 1990.

Cande, S. C., and D. V. Kent, A new geomagnetic polarity timescale for the Late Cretaceous and Cenozoic, *J. Geophys. Res.*, *97*, 13,917–13,951, 1992.

Carlson, R. L., and C. N. Herrick, Densities and porosities in the oceanic crust and their variations with depth and age, *J. Geophys. Res.*, *95*, 9153–9170, 1990.

Cox, K. G., A model for flood basalt volcanism, *J. Petrol.*, *21*, 629–650, 1980.

Fowler, S. R., R. S. White, G. D. Spence, and G.K. Westbrook, The Hatton Bank continental margin–II. Deep

structure from two-ship expanding spread seismic profiles, *Geophys. J., 96*, 295–309, 1989.

Furlong, K. P, and D. M. Fountain, Continental crustal underplating: Thermal considerations and seismo-petrologic consequences, *J. Geophys. Res., 91*, 8285–8294, 1986.

Goldschmidt-Rokita, A., K. J. F. Hansch, H. B. Hirschleber, T. Iwasaki, T. Kanazawa, H. Shimamura, and M. A. Sellevol, The ocean/continent transition along a profile through the Lofoten Basin, northern Norway, *Mar. Geophys. Res., 16*, 201–224, 1994.

Hinz, K., A hypothesis on terrestrial catastrophes: Wedges of very thick oceanward dipping layers beneath passive continental margins–Their origin and paleoenvironmental significance, *Geol. Jahrb., Reiche E, 22*, 2–28, 1981.

Holbrook, W. S., and P. B. Kelemen, Large igneous province on the U.S. Atlantic margin and implications for magmatism during continental breakup, *Nature, 364*, 433-436, 1993.

Holbrook, W. S., E. C. Reiter, G. M. Purdy, D. Sawyer, P. L. Stoffa, J. A. Austin, J. Oh, and J. Makris, Deep structure of the U.S. Atlantic continental margin, offshore Carolina, from coincident ocean bottom and multichannel seismic data, *J. Geophys. Res., 99*, 9155–9174, 1994.

Horsefield, S. J., R. B. Whitmarsh, R. S. White, and J.-C. Sibuet, Crustal structure of the Goban Spur rifted continental margin, *Geophys. J. Int., 119*, 1–19, 1994.

Houseman, G. A., The thermal structure of mantle plumes: Axisymmetric or triple-junction?, *Geophys. J. Int., 102*, 15–24, 1990.

Jones, E. J. W., R. S. White, V. J. Hughes, D. H. Matthews, and B. R. Clayton, Crustal structure of the continental shelf of NW Britain from two-ship seismic experiments, *Geophysics, 49*, 1605–1621, 1984.

Kelemen, P. B., and W. S. Holbrook, Origin of thick, high-velocity igneous crust along the U.S. East Coast margin, *J. Geophys. Res., 100*, 10,077–10,094, 1995.

Kodaira, S., A. Goldschmidt-Rokita, J. M. Hartmann, H. B. Hirschleber, T. Iwasaki, T. Kanazawa, H. Krahn, S. Tomita, and H. Shimamura, Crustal structure of the Lofoten continental-margin, off northern Norway, from ocean-bottom seismographic studies, *Geophys. J. Int., 121*, 907–924, 1995.

Larsen, H. C., and S. Jakobsdóttir, Distribution, crustal properties and significance of seaward dipping subbasement reflectors off east Greenland, in *Early Tertiary Volcanism and the Opening of the NE Atlantic*, edited by A. C. Morton and L. M. Parson, *Geol. Soc. Spec. Publ., 39*, 95–114, 1988.

LASE Study Group, Deep structure of the U.S. East Coast passive margin from large aperture seismic experiments (LASE), *Mar. Pet. Geol., 3*, 234–242, 1986.

LeCheminant, A. N., and L. M. Heaman, Mackenzie igneous events, Canada: Middle Proterozoic hotspot magmatism associated with ocean opening, *Earth Planet. Sci. Lett., 96*, 38–48, 1989.

Lister, J. R., and R. C. Kerr, Fluid-mechanical models of crack propagation and their application to magma transport in dykes, *J. Geophys. Res., 96*, 10,049–10,077, 1991.

Makris, J., K. Lange, L. Savostin, and V. Sedov, A wide-angle reflection profile across the Iceland-Faeroe Ridge, in *The Petroleum Geology of Ireland's Offshore Basins*, edited by P. F. Croker, and P. M. Shannon, *Geol. Soc. Spec. Publ., 93*, 459–466, 1995.

McBride, J. H., T. J. Henstock, R. S. White, and R. W. Hobbs, Seismic reflection profiling in deep water: Avoiding spurious reflectivity at lower-crustal and upper-mantle traveltimes, *Tectonophysics, 232*, 425–435, 1994.

Mjelde, R., M. A. Sellevol, H. Shimamura, T. Iwasaki, and T. Kanazawa, A crustal study off Lofoten, N. Norway, by use of 3-component ocean bottom seismographs, *Tectonophysics, 212*, 269–288, 1992.

Morgan, J., P. J. Barton, and R. S. White, The Hatton Bank continental margin, III, Structure from wide-angle OBS and multichannel seismic refraction profiles, *Geophys. J. Int., 89*, 367–384, 1989.

Morton, A. C., and P. N. Taylor, Lead isotope evidence for the structure of the Rockall dipping reflector passive margin, *Nature, 326*, 381–383, 1987.

Murray, J. W., Paleogene and Neogene benthic foraminiferas from Rockall Plateau, *Initial Rep. Deep Sea Drill. Proj., 81*, 503–534, 1984.

Mutter, J. C., and C. M. Zehnder, Deep crustal structure and magmatic processes: The inception of seafloor spreading in the Norwegian-Greenland Sea, in *Early Tertiary Volcanism and the Opening of the NE Atlantic*, edited by A. C. Morton and L. M. Parson, *Geol. Soc. Spec. Publ., 39*, 35–48, 1988.

Mutter, J. C., W. R. Buck, and C. M. Zehnder, Convective partial melting, 1, A model for the formation of thick basaltic sequences during the initiation of spreading, *J. Geophys. Res., 93*, 1031–1048, 1988.

Nafe, J. E., and C. L. Drake, Variation with depth in shallow and deep water marine sediments of porosity, density and the velocities of compressional and shear waves, *Geophysics, 22*, 523–552, 1957.

Olafsson, I., E. Sundvor, O. Eldholm and K. Grue, Møre margin: Crustal structure from analysis of ESPs. *Mar. Geophys. Res., 14*, 137–162, 1992.

Oxburgh, E. R., and E. M. Parmentier, Compositional and density stratification in oceanic lithosphere – Causes and consequences, *J. Geol. Soc. London, 133*, 343–355, 1977.

Pálmason, G., A continuum model of crustal generation in Iceland: Kinematic aspects, *J. Geophys., 47*, 7–18, 1980.

Planke, S., and O. Eldholm, Seismic response and construction of seaward dipping reflectors in flood basalts: Vøring volcanic margin, *J. Geophys. Res., 99*, 9263–9278, 1994.

Powell, C. M. R., A wide-angle multichannel seismic study of the continental lithosphere, Ph.D. dissertation, Univ. of Cambridge, Cambridge, England, 1986.

Prescott, C. N., Marine geophysical investigations of the Hatton Bank volcanic passive continental margin, Ph.D. dissertation, Univ. of Durham, Durham, England, 1988.

Richards, M. A., R. A. Duncan, and V. E. Courtillot, Flood basalts and hotspot tracks: Plume heads and tails, *Science, 246*, 103–107, 1989.

Roberts, D. G., J. Backman, A. C. Morton, J. W. Murray, and J. B. Keene, Evolution of volcanic rifted margins: Synthesis of Leg 81 results on the west margin of Rockall Plateau, *Initial Rep. Deep Sea Drill. Proj., 81*, 883–912, 1984.

Scrutton, R., The structure of the Rockall microcontinent, *Geophys. J. R. Astron. Soc., 27*, 259–275, 1972.

Sheridan, R. E., D. L. Musser, L. Glover III, M. Talwani, J. Ewing, W. S. Holbrook, G. M. Purdy, R. Hawman, and S. Smithson, Deep seismic reflection data of the EDGE U.S. Mid-Atlantic continental margin experiment: Implications for Appalachian sutures, Mesozoic rifting and magmatic underplating, *Geology, 21*, 563–567, 1993.

Sigurdsson, H., and R. S. J. Sparks, Lateral magma flow within rifted Icelandic crust, *Nature, 274*, 126–130, 1978.

Smythe, D. K., Rockall Trough–Cretaceous or Late Palaeozoic?, *Scott. J. Geol., 25*, 5–43, 1989.

Spence, G. D., R. S. White, G. K. Westbrook, and S. R. Fowler, The Hatton Bank continental margin, I, Shallow structure from two-ship expanding spread seismic profiles, *Geophys. J., 96*, 273–294, 1989.

Srivastava, S. P., Evolution of the Labrador Sea and its bear-

ing on the early evolution of the North Atlantic, *Geophys. J. R. Astron. Soc., 52*, 313–355, 1978.

Tréhu, A. M., A. Ballard, L. M. Dorman, J. F. Gettrust, K. D. Klitgord, and A. Shreiner, Structure of the lower crust beneath the Carolina Trough, U.S. Atlantic continental margin, *J. Geophys. Res., 94*, 10,585–10,600, 1989.

White, R. S., Crustal structure and magmatism of North Atlantic continental margins, *J. Geol. Soc. London, 149*, 841–853, 1992.

White, R., and D. McKenzie, Magmatism at rift zones: The generation of volcanic continental margins and flood basalts, *J. Geophys. Res., 94*, 7685–7729, 1989.

White, R. S., and D. McKenzie, Mantle plumes and flood basalts, *J. Geophys. Res., 100*, 17,543–17,585, 1995.

White, R. S., G. D. Spence, S. R. Fowler, D. P. McKenzie, G. K. Westbrook, and A. N. Bowen, Magmatism at rifted continental margins, *Nature, 330*, 439–444, 1987.

White, R. S., D. McKenzie, and R. K. O'Nions, Oceanic crustal thickness from seismic measurements and rare earth element inversions, *J. Geophys. Res., 97*, 19,683–19,715, 1992.

White, R. S., J. W. Bown, and J. R. Smallwood, The temperature of the Iceland plume and origin of outward-propagating V-shaped ridges, *J. Geol. Soc. London, 152*, 1039–1045, 1995.

Zelt, C. A., and R. B. Smith, Seismic traveltime inversion for 2-D crustal velocity structure, *Geophys. J. Int., 108*, 16–34, 1992.

A. J. Barton and R. S. White, Bullard Laboratories, Department of Earth Sciences, University of Cambridge, Madingley Road, Cambridge CB3 0EZ, England. (e-mail: rwhite@esc.cam.ac.uk)

(Received February 7, 1996; revised October 23, 1996; accepted October 30, 1996.)